NREL/TP-411-6396 • UC Category: 271 • DE94000298

Research on Stable, High-Efficiency Amorphous Silicon Multijunction Modules

Semiannual Subcontract Report
1 March 1993 – 30 November 1993

S. Guha
United Solar Systems Corporation
Troy, Michigan

NREL technical monitor: W. Luft

National Renewable Energy Laboratory
1617 Cole Boulevard
Golden, Colorado 80401-3393
A national laboratory of the U.S. Department of Energy
Operated by Midwest Research Institute
for the U.S. Department of Energy
under contract No. DE-AC02-83CH10093

Prepared under Subcontract No. ZM-1-19033-2

March 1994

NOTICE

Printed in the United States of America
Available from:
National Technical Information Service
U.S. Department of Commerce
5285 Port Royal Road
Springfield, VA 22161

Price: Microfiche A01
Printed Copy A04

Codes are used for pricing all publications. The code is determined by the number of pages in the publication. Information pertaining to the pricing codes can be found in the current issue of the following publications which are generally available in most libraries: *Energy Research Abstracts (ERA); Government Reports Announcements and Index (GRA and I); Scientific and Technical Abstract Reports (STAR)*; and publication NTIS-PR-360 available from NTIS at the above address.

Printed on recycled paper

Preface

This Semiannual Subcontract Report covers the work performed by United Solar Systems Corp. for the period 1 March 1993 to 30 November 1993 under DOE/NREL Subcontract Number ZM-1-19033-2. The following personnel participated in the research program.

> A. Banerjee, E. Chen, R. Clough, T. Glatfelter, S. Guha (Principal Investigator), G. Hammond, K. Hoffman, M. Hopson, N. Jackett, M. Lycette, J. Noch, T. Palmer, K. Parker, I. Rosenstein, D. Wolf, J. Yang, X. Xu and K. Younan.

The small-angle X-ray scattering experiments reported in Section 3 were carried out at the Colorado School of Mines by D. L. Williamson, S. J. Jones and Y. Chen, and we thank them for this collaborative effort.

We would like to thank V. Trudeau for preparation of this report.

Table of Contents

List of Figures

Page

List of Tables

Executive Summary

Objectives

The principal objective of the program is to conduct research on semiconductor materials and non-semiconductor materials to enhance the performance of multi-bandgap, multijunction, large-area amorphous silicon-based alloy modules. The goal for Phase III is to demonstrate stabilized module efficiency of 12% for multijunction panel of area greater than 900 cm^2.

Approach

Double-junction and triple-junction cells are made on Ag/ZnO back reflector deposited on stainless steel substrates. a-SiGe alloy is used for the i-layer in the bottom and the middle cells; the top cell uses a-Si alloy. After evaporation of antireflection coating, silver grids and bus bars are put on the top surface, and the panel is encapsulated in an ethylene vinyl acetate (EVA)/Tefzel structure to make a one-square-foot monolithic module.

Status/Accomplishments

- Detailed optical modeling studies have been conducted to identify parasitic optical losses in solar cells on textured back reflectors.
- Component cells in a multijunction structure have been optimized to obtain higher stabilized efficiencies under the relevant light spectrum.
- The role of microstructure in amorphous silicon-germanium films on cell performance has been investigated.
- A large number of double-junction modules have been made with aperture area larger than 900 cm^2 showing initial efficiencies higher than 11%. The highest initial efficiency of our modules as measured by NREL is 11.4%. **This is the highest efficiency confirmed by NREL for any thin-film module.** A double-junction module with an initial efficiency of 11.1% showed a stabilized efficiency of 9.5% after 1000 h of one-sun light soaking.

Section 1

Introduction

The research program is directed toward advancing our understanding of amorphous silicon alloys and other relevant non-semiconductor materials for use in large-area multijunction modules. An important thrust of the program is on performance of modules after long-time light exposure; therefore, study of light-induced degradation forms an important part of the program. The goal of this phase of the program is to demonstrate a stable, aperture-area efficiency of 12% for a two-terminal, multi-bandgap, multijunction module of aperture area of at least 900 cm^2.

The program is divided into three tasks. Task I, semiconductor materials research, is directed toward depositing, optimizing and characterizing of suitable amorphous silicon alloy materials and cell structures over 900 cm^2. Task 2, non-semiconductor materials research, involves investigating suitable back reflectors and antireflection coatings and also encapsulants for the modules. Task 3, module research, is directed toward fabricating modules involving grid patterning, cell isolation and interconnect, and encapsulation.

In this report, we outline the progress made toward the program goal in the different task areas. In Section 2, we describe results from our optical modeling work where we analyze the effect of light-trapping on quantum efficiency and short-circuit current density of cells deposited on textured back reflector. Comparing the results of the modeling with experimental data, we show that parasitic optical loss (probably associated with the textured silver/zinc oxide back reflector) limits the gain in short-circuit current density that could be achieved from light trapping. In Section 3, we present data on the component cells of the multijunction structure. We demonstrate the improvement of the performance of the top cell with the use of hydrogen dilution during deposition. We also investigate the effect of microstructure on the performance of amorphous silicon-germanium alloy solar cells. In Section 4, we discuss the status of our large-area deposition work. Significant progress has been made on the performance of component cells which resulted in higher efficiency for double-junction modules. The highest initial efficiency on a one-square-foot module as confirmed by NREL was 11.4%. This is the highest efficiency confirmed by NREL for any thin film module. After one-sun light soaking for 1000 h, a module with an initial efficiency of 11.1% stabilized at 9.5%. In Section 5, we discuss the spectral corrections necessary to obtain global AM1.5 performance of modules based on outdoor measurements. Summary of the work and future directions are outlined in Section 6.

Section 2

Optical Modeling

Introduction

We have been engaged in a continuing effort to better understand the optical performance of our solar cells. Previously, a method was formulated which can characterize the thickness, index of refraction and optical absorption of the individual layers comprising a complete solar cell.[1,2] This procedure is based on coherent optics; therefore it is unable to accurately model solar cells grown on textured substrates. Of course, textured and reflection enhanced substrates are desirable for amplifying the short-circuit current. In this section, we will convey the progress that has been made to optically characterize solar cells fabricated on textured substrates.

The work on specular substrates revealed unexpected parasitic optical absorptions.[2] While these losses were of small consequence for cells grown on flat substrates, it is probable that their influence is greater on light scattering surfaces. In the present effort, we have been able to estimate the effect of parasitic losses for solar cells made on light trapping (i.e., textured) substrates. We have also been able to represent the positive impact that a so-called "perfect" substrate would have in conjunction with our solar cells. These ideas will be presented here. We have also performed some preliminary efforts to match measured spectral response and reflection data to calculations, which will also be outlined herein. In addition, certain questions related to the measurements and calculations described in this section can be formulated. These represent unknowns and anomalies that will be considered for speculation and future efforts.

Modeling and Measurement Tools

As was true for specular modeling, we would like to use standard solar cell optical measurements to interface calculations to real data. This includes spectral response and reflection spectra. Reflection measurements are more difficult when using scattered light. Thus, we designed and built a large-area integrating sphere detector in order to accurately measure the absolute reflection as a function of the wavelength of the incident light. This is coupled to a spectral response system, sharing the monochromator and much of the optical apparatus with it. Measurements of highly diffuse calibration reflection standards reveal that it accurately measures the reflection ± 0.5% over each band of the whole measured spectrum range (350 - 950 nm). We have also constructed an apparatus that is capable of measuring reflected light as a function of scattering angle. These measurements are obtained using a He-Ne laser at 633 nm.

There exist two FORTRAN 77 compiled computer programs that were used in this study. The first program was formulated at USSC and is based on the coherent optics algorithm mentioned above. Its foundation has been described in detail before.[1,2] Briefly, this program uses a simplex optimization routine to adjust the optical constants of individual layers in a solar cell stack in order to iteratively match measured spectral response and reflection spectra. It will be referred to in this report as QFIT. The second computer program was developed at Georgia Tech Research Institute. A description of the principles of this algorithm is also in the literature.[3] In short, it is a Monte Carlo ray tracing program that can numerically simulate the light trapping due to various textures on the top and/or bottom surfaces of a solar cell. It will be referred to in this text as TEXTURE.

Analysis of Textured Substrate Performance

A "figure of merit" that can be used to assess the performance of a light trapping system is the enhancement factor (E.F.). The E.F. is defined as the increase in the effective absorption due to light trapping. It has been shown that when light within a material is randomized, there is a thermodynamic limit for the absorption increase[4] that is

$$\text{E.F. (max.)} = 4 \times n^2 \text{, where n is the refractive index} \qquad (1)$$

For the case of amorphous silicon-based solar cells, this number is about 50 in reddish light. For amorphous silicon-germanium alloy solar cells, E.F. (max.) is approximately 60. In general, there are two factors that tend to prevent a solar cell designer from obtaining the theoretical limit of Eq. (1): i) Parasitic optical losses and ii) non-randomized photons. The first item encompasses several causes including, but not necessarily limited to, absorption from the semiconductor dopant layers, absorption in the metal oxide layers (refer to Fig. 1), interface absorption, and, possibly, absorption due to the geometry of the texturing.[5] Lack of light randomization could arise from "imperfect" texturing of the substrate. In our laboratory, we often can measure a specular component in our textured substrates. Also, we have seen coherent structure in the spectra due to light scattering angle.

Figure 2 illustrates some analysis of the light trapping on amorphous silicon-based solar cells. This is a plot of calculated and measured E.F. for 3 sets of cells whose intrinsic layer thicknesses were nominally 230, 460, and 920 nm, a 1:2:4 ratio. The curves marked "Actual Cell Data" were obtained in the following manner. Each of the three cells was deposited using identical conditions onto both stainless steel and textured substrates. The cells were made using state-of-art materials from USSC's LINE machine. The intrinsic layer thickness differences were obtained by varying the deposition time of the intrinsic layer using the 1:2:4 ratio. The textured substrates consist of stainless steel coated with silver and then subsequently zinc oxide via sputtering. The silver and zinc oxide deposition conditions were adjusted to achieve certain desirable texturing that empirically resulted in maximizing the solar conversion efficiency. The spectral response and reflection versus wavelength of the cells deposited on bare steel were obtained, and the cells were modeled using QFIT. Thus, the absorption coefficients of the intrinsic layers were gleaned. The effective absorption coefficients were acquired from the spectral response of cells deposited onto textured substrates. The ratio of these absorption values to the absorption values from the QFIT simulation is the E.F.

TEXTURE calculated enhancement factors for the 3 cells under two separate conditions: 100% back surface reflection and 90% back surface reflection. The textured case was simulated by using pure Lambertian scattering at both the top and bottom surfaces. Incidentally, it has been found that either surface may be specular and achieve the same results, which implies that one Lambertian surface is able to completely randomize the light. The absorption values of the intrinsic layer used in this calculation were made to be the same as those calculated with QFIT. The results of these efforts for each of the 3 cells are plotted in Fig. 2. The outcome of Eq. (1) is also plotted in the figure for comparison.

Some tentative observations and conclusions can be made by putting Fig. 2 under scrutiny. A small total parasitic loss in the light trapping system can cause a large drop in the E.F.; Fig. 2 reveals that a 10% optical loss reduces the E.F. about 50%. The E.F. of USSC's cells is much smaller than the theoretical values. This may indicate that there is considerable scope for improvement. The decrease in the E.F. of the actual data at higher wavelengths is not completely understood. It may be due to the fact that the absorption values obtained from QFIT at long wavelengths are somewhat incorrect. The spectral response at these wavelengths is very small (less than 1%) so that the semiconductor model inside the QFIT engine may not be able to accurately determine the absorption. Also, the reader may have noticed that the 100%

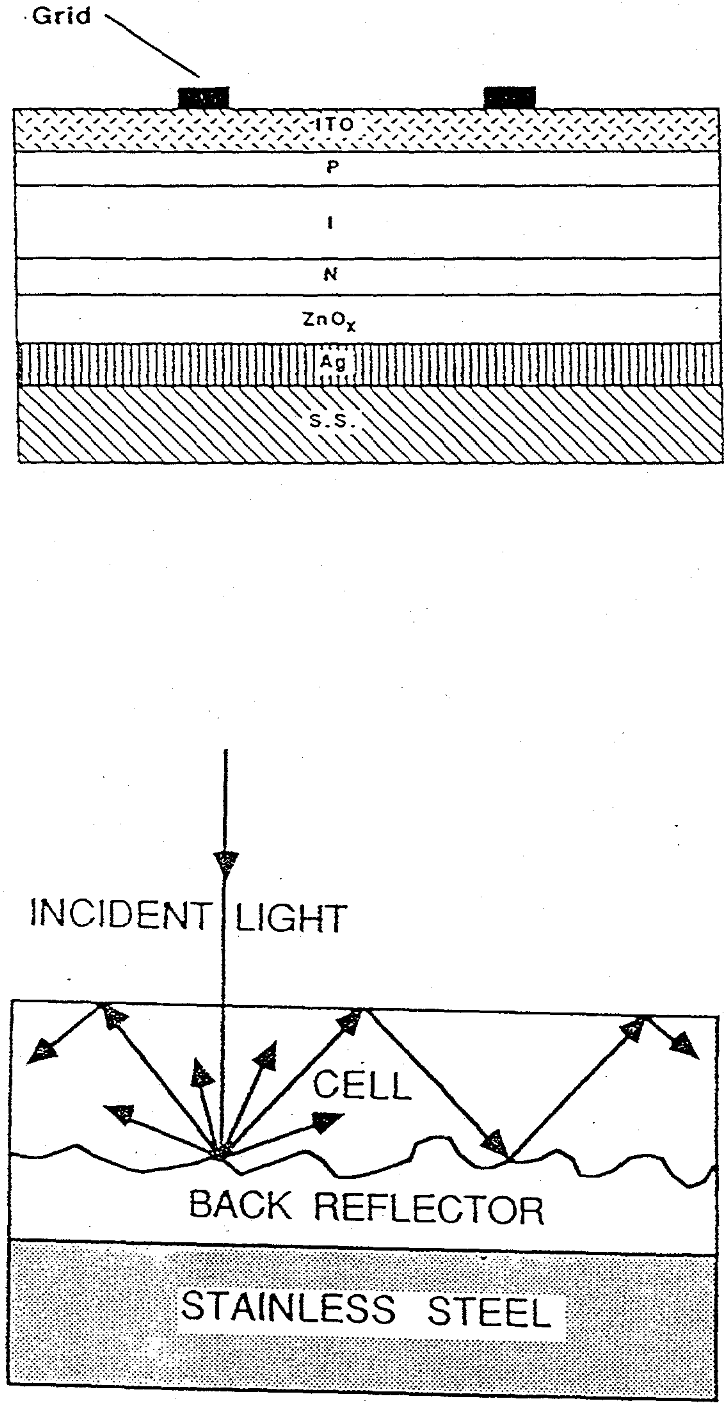

Figure 1. Representation of the structure of solar cells fabricated on textured substrates used in this study.

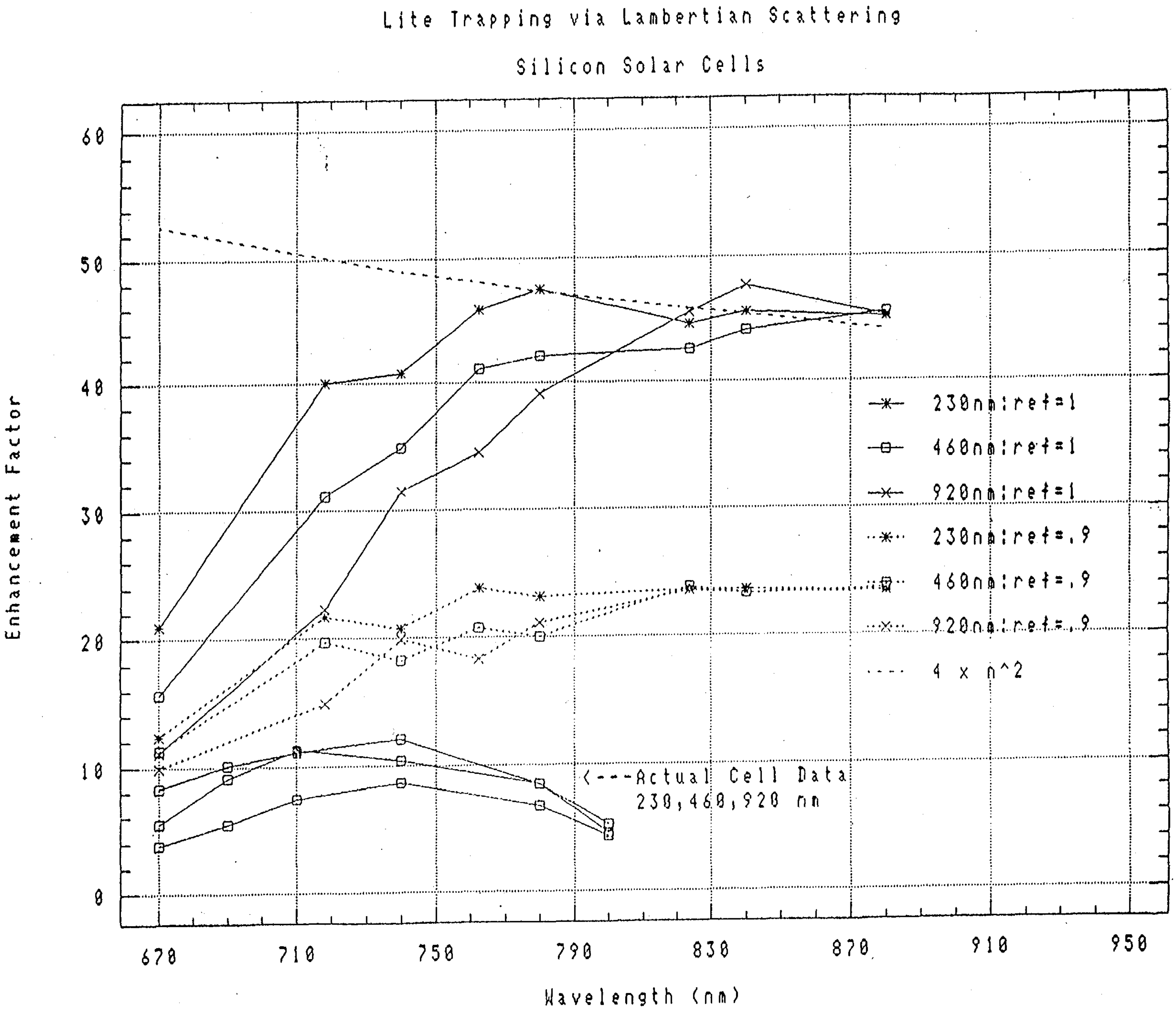

using absorption from exp.

Figure 2. Enhancement Factor versus Wavelength of incident light for 3 a-Si:H solar cells. Calculations and experimental data are included on this chart. The representations are described in the text.

texture calculation is lower than 4 x n^2 at the lower wavelength region of Fig. 2. This is because Eq. (1) is valid when the light is uniformly absorbed, which is not true unless the absorption coefficient is reasonably small.

Figure 3 depicts again some of the curves from Fig. 2 but includes similar data for an amorphous silicon-germanium alloy solar cell. The intrinsic layer of the a-Si:Ge cell has a bandgap of 1.43 eV. The higher values of E.F. for this cell when compared to an a-Si cell can be noted. This is true for both data and calculation. Eq. (1) indicates that the higher E.F. for the germanium case is to be expected. Fig. 3 only includes the 100% reflection case for clarity.

While the portrayal of the E.F. effects reveal much about what is going on optically, the solar cell designer needs to know the "bottom line." What is the effect on Jsc, the short-circuit current? Figure 4 illustrates the answer. The silicon-germanium alloy cells from Fig. 3 are depicted here anew. The figure shows the measured spectral response of the cell on bare steel, the cell on the textured substrate, and the TEXTURE calculation of this cell without losses. Integration of these curves with respect to the AM1.5 Global Standard Solar Insolation demonstrates that the gain due to the present substrate is about 5.5 mA/cm^2. The additional gain that is apparently theoretically possible is 4.5 mA/cm^2!

Spectral Response and Reflection of Textured Solar Cells

An attempt has been made to calculate both the spectral response and the global reflection for a certain solar cell fabricated on a textured substrate. The only adjustable parameter varied to fit the data was the parasitic optical loss. The specular component of the textured substrate was measured prior to the semiconductor depositions. The measurement was performed with a detector situated normal to a reflected laser spot. The detector subtended a very small solid angle of less than 0.01%. The incident light struck the sample about 6° from the perpendicular normal. The resulting value of 20.7% specularity was used in the calculations represented in the discussion following to weight the specular against the textured components of the spectral response and reflection. The thicknesses and optical constants for each layer of the solar cell were obtained using QFIT from an identical cell deposited on bare stainless steel. QFIT was then used to recalculate the spectral response and reflection spectra of this cell while inserting silver and zinc oxide layers into the modeled optical stack (as in Fig. 1). The optical constants for the silver were obtained previously from ellipsometry. The indices of refraction for the zinc oxide came from ellipsometry also, but the extinction coefficient was artificially inserted to correspond to certain back surface parasitic losses. During the recalculation, the thickness of the intrinsic layer was adjusted so that the calculated maxima and minima in the reflection spectra matched the measured maxima and minima of the textured solar cell. This had the effect of adjusting the deposition thickness of the flat case to correspond to the textured case. In this instance, it was found that the intrinsic layer is optically 20% thinner when deposited on this particular textured substrate than when it was deposited on the flat stainless steel substrate. When these adjustments were completed, the result represents the specular component of the modeled solar cell.

The textured component of the spectral response and reflection for this solar cell under consideration was made using TEXTURE. The intrinsic layer optical constants were obtained from QFIT as described above. TEXTURE repeated these calculations for several back surface parasitic losses, corresponding to the losses used for the specular situation. Finally, the specular component of both the reflection and spectral response was weighted at 20.7%, while the textured elements were weighted at 79.3%. The weightings correspond to the measured specularity of the base substrate. The resulting spectral response curves for these calculations are plotted in Fig. 5 with the actual measured data. Similarly, the reflection calculations and data are represented in Fig. 6.

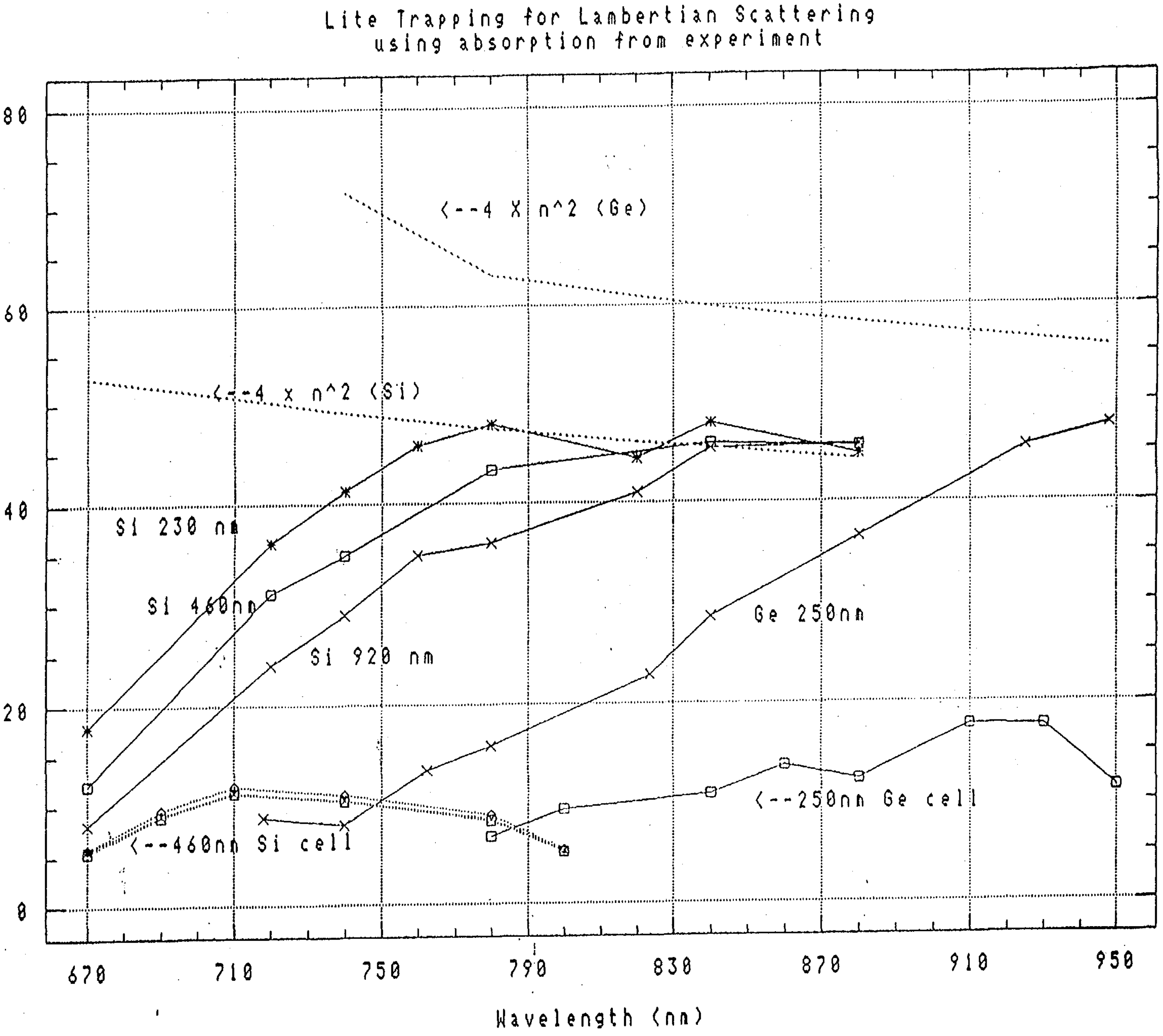

TEXTURE program

Figure 3. Enhancement Factor versus Wavelength of Incident light for a-Si:H and a-Si:Ge:H solar cells. Calculations and experimental data are included on this chart. The representations are described in the text.

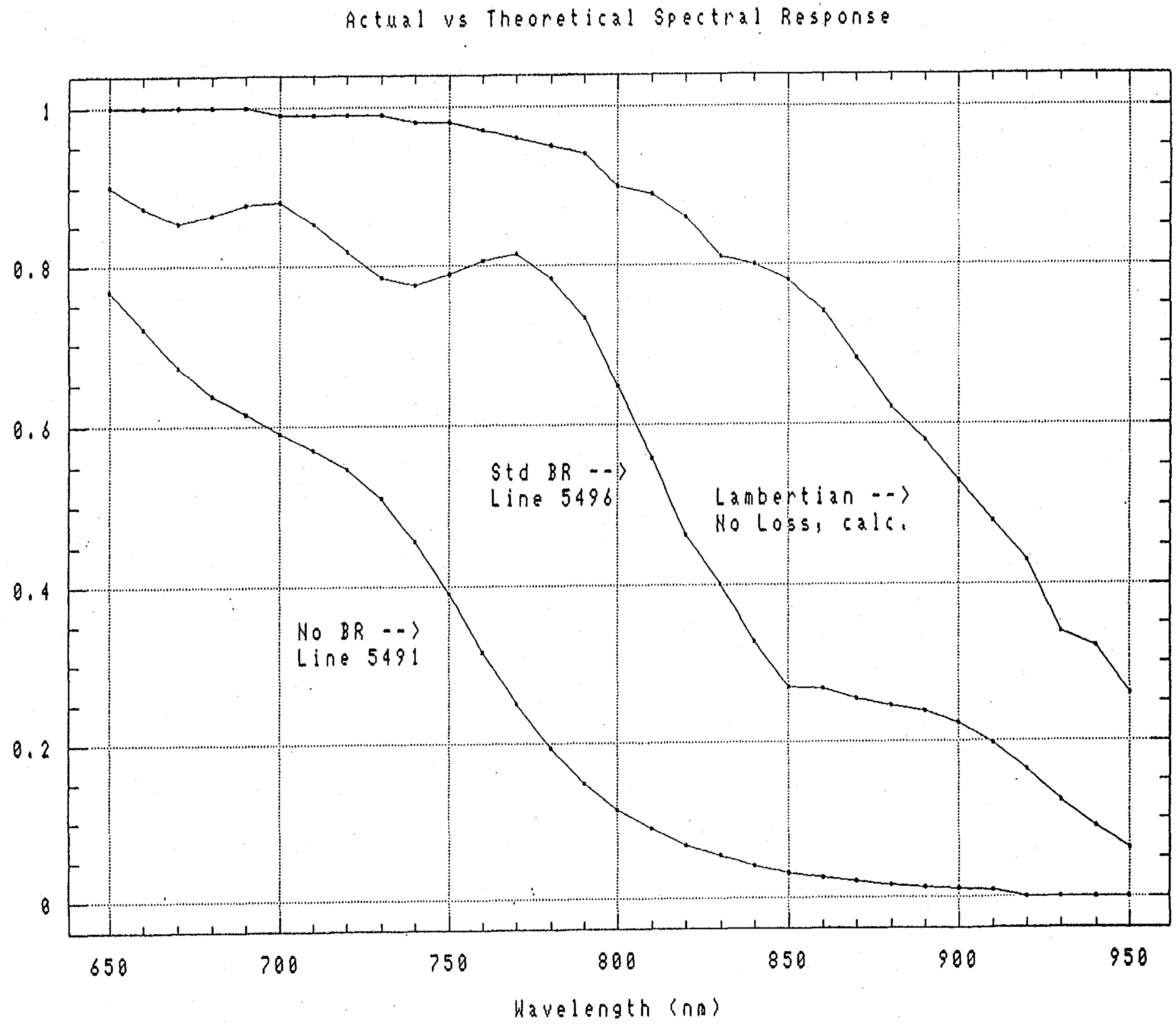

2,500 Angstrom

Figure 4. Spectral Response versus Wavelength of incident light. The curves labeled Line 5491 and Line 5496 are obtained from measurements. The third curve is due to a calculation using an ideal textured substrate.

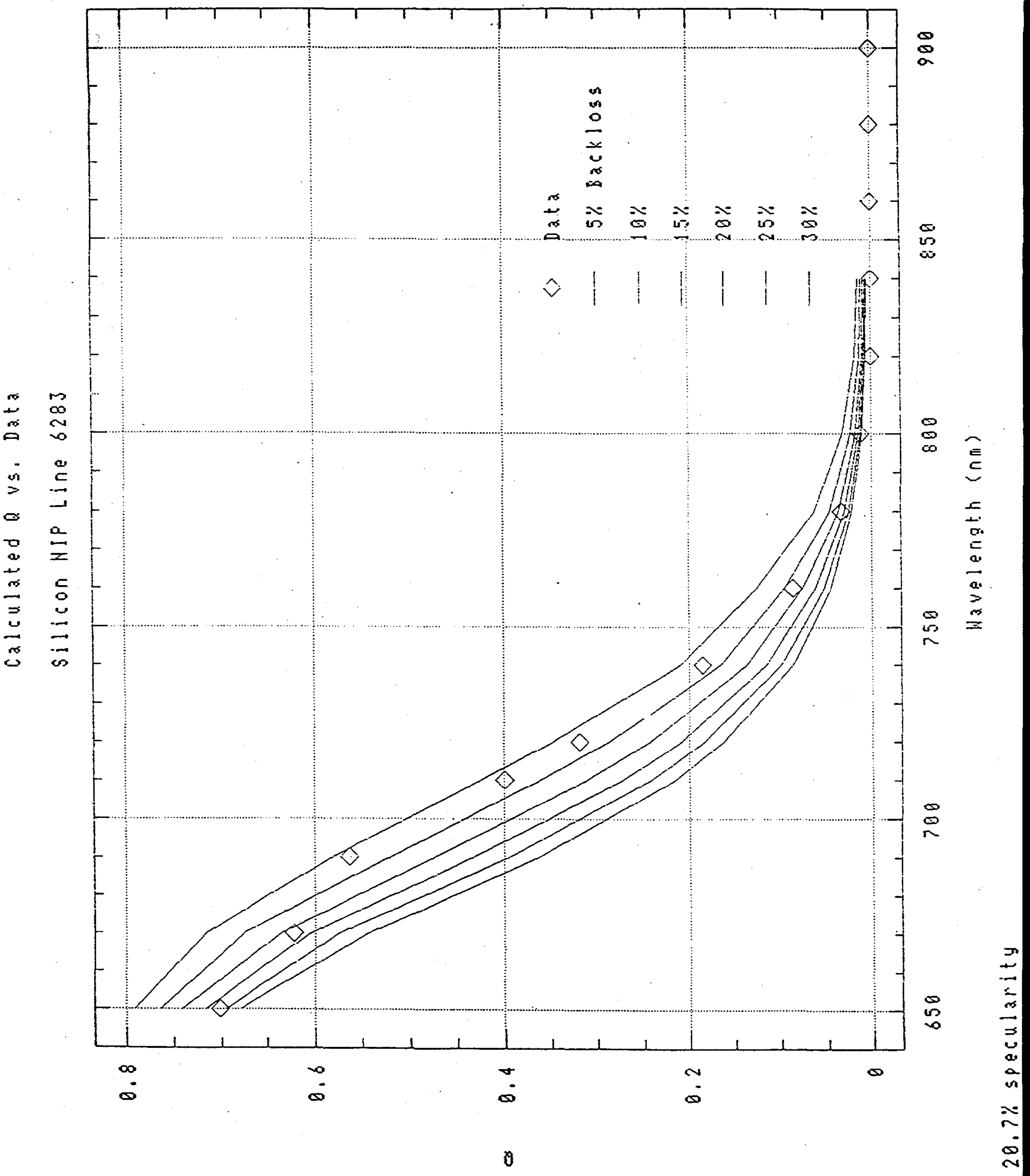

Figure 5. Spectral Response versus Wavelength of incident light for an a-Si:H solar cell. Measured data are represented by the diamond. The 6 curves are calculations using indicated back surface losses.

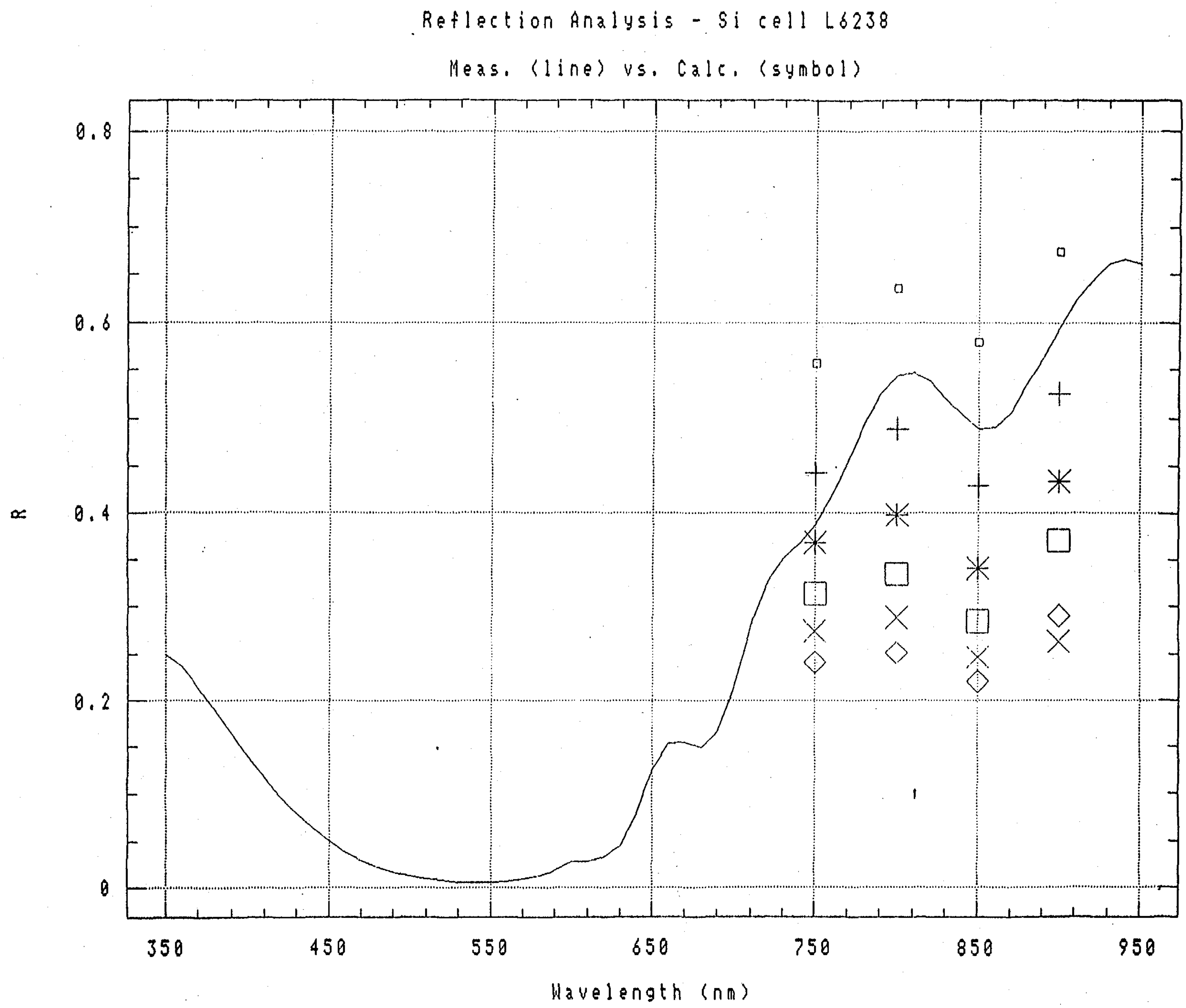

assumes 20.7% ref calc.

Figure 6. Global Reflection versus Wavelength of incident light for the solar cell of Fig. 5. Measured data are represented by the solid line. The symbols represent calculations using the same back surface losses as in Fig. 5.

Both Figs. 5 and 6 indicate a good fit with a back reflector loss of about 10%. The structure in the spectral response data of Fig. 5, presumably due to coherence, was not emulated in the calculations. This suggests that a significant portion of the scattered light is coherent. Measurement of the reflection versus scattering angle for this substrate does, in fact, have structure at angles less than 30°. On the other hand, the structure of the reflection revealed in Fig. 6 seems to be modeled well. Unfortunately, this modeling attempt does not clearly answer the question of whether or not this light trapping technology can be simulated using geometric optics.

Additional Observations

Reflection measurements of solar cells on textured substrates have raised some problematic issues. This is particularly so in view of the fact that our laboratory's global reflection measurement apparatus has been improved. For example, the textured substrates typically have reflection values of only 90%, despite the fact that the silver base has been measured repeatedly to be about 98% and the metal oxide is found to have very little absorption. Another example, the sum of the spectral response and reflection (and the reflection in the near infrared), is about 70% at best. Where is the missing light? A substrate was made as part of this effort that had a specular component of 0% and a measured reflection of about 90%, but the resulting solar cells had inferior spectral responses. This appears anomalous when compared to some of the other evidence. The testimony of the work reported in this section seems to point toward the possibility that a large amount of light is lost due to parasitic optical absorption. However, many attempts at isolating such losses have not born fruit. We plan to continue these efforts until a thorough understanding of the light trapping system is realized and the consequential improvement in solar cell performance is realized.

Section 3

Materials and Cell Research

Introduction

In order to obtain high efficiency multijunction cells, it is necessary to optimize the component cell deposition conditions. In this section, we present data on the effect of hydrogen dilution on the characteristics of the top cell and show that the stabilized efficiency of the cell improves as a result of hydrogen dilution. We also present the current status of stabilized performance of the middle and the bottom cells. We have also investigated the influence of microstructure on the performance of a-SiGe alloy cells in the initial and light-soaked conditions. Unlike the use of a-Si alloys, we do not observe good correlation between microstructure and cell properties. Finally, we present experimental results on light soaking of double- and triple-junction cells under a metal arc lamp and a global AM1.5 source. Although the spectra of the two sources are quite different, we find the degradation of the cells to be quite similar.

Wide Bandgap Amorphous Silicon Alloy Top Cell

Based on our recent study on the light-induced degradation of component cells of a multijunction structure, a 10-18% degradation is expected for a typical state-of-the-art triple-junction device.[6] The top cell, which is thin but exposed to full sunlight, degraded by 10-12%, half of which is due to degradation in V_{oc}, the open-circuit voltage. Since the multijunction cells are designed to be top cell limited, any improvement in the initial efficiency or stability of the top cell will result in a higher performance in the multijunction structure.

One approach to improve the top cell is to incorporate wide-bandgap a-SiC:H alloy for the intrinsic layer to enhance V_{oc}. However, this approach often resulted in a poorer fill factor or larger degradation than using conventional a-Si:H materials, although some recent data reported improved performance.[7] In this section, we show that by increasing hydrogen dilution and optimizing deposition conditions without incorporation of carbon, one can improve the top cell performance both in terms of initial efficiency and stability.

Typical initial and degraded performance for our "standard" top cell is shown in Table 1. Sample A is made using conventional rf deposition conditions[8] on stainless steel substrate without any back reflector. The short-circuit current density, J_{sc}, of ~ 7 mA/cm^2 without a back reflector is well suited for the top cell of a triple-junction structure. Light soaking was carried out using one-sun illumination with a metal-arc lamp for 1800 hours at 50°C under open-circuit condition. As pointed out earlier, light soaking causes a degradation of about 50 mV in V_{oc}. In order to understand if the V_{oc} degradation is caused by bulk or interface effects, light soaking experiments were carried out with light sources having different spectra so as to obtain different generation profiles in the device. Two groups of devices selected from the same sample were illuminated under blue light (with a 550 nm cut-off filter) and red light (with a 610 nm cut-on filter), respectively, for 30 minutes at 34°C. The light intensity in both cases was adjusted so that J_{sc} is equal to that obtained for 8 suns. The results are shown in Table 2. Very similar degradation in V_{oc}, in the range of 34-39 mV, was observed in the two cases. Since blue light is predominately absorbed near the interface whereas red light is absorbed more uniformly in the bulk, the above results indicate that the degradation at the interface is not more severe than in the bulk. Theoretical calculation based on numerical model developed in our group[9] for single and multijunction cells indicate a drop of about 50 mV in V_{oc} of a 1000 Å thick cell, if the minimum gap state density in the bulk goes up by a factor of

Table 1. **Characteristics of "Standard" and "Improved" Top Cells in Both Initial and Degraded States.**

		J_{sc} (mA/cm^2)	V_{oc} (V)	FF	P_{max} (mW/cm^2)
Sample A ("standard")	Initial	7.1	0.97	0.76	5.23
	Degraded	7.1	0.92	0.70	4.57
	Degradation (%)	0	5.2	7.9	12.6
Sample B ("improved")	Initial	7.3	1.01	0.75	5.53
	Degraded	7.2	0.98	0.71	5.01
	Degradation (%)	1.4	3.0	5.3	9.4

Table 2. **Characteristics of "Standard" Top Cells in Both Initial and Degraded States.**

Light Soaking Spectrum	State	J_{sc} (mA/cm^2)	V_{oc} (V)	FF	P_{max} (mW/cm^2)
Red (610 nm cut-on)	Initial	10.20	0.948	0.718	6.93
	Degraded	9.99	0.914	0.624	5.70
	Degradation (%)	2.0	3.6	13.1	17.8
Blue (550 nm cut-off)	Initial	10.32	0.954	0.726	7.14
	Degraded	10.05	0.915	0.613	5.63
	Degradation (%)	2.6	4.1	15.6	21.1

4 from 5×10^{15} to 2×10^{16} $cm^{-3} eV^{-1}$. Because these are very reasonable numbers based on other estimates[10] on device quality materials, we conclude that the performance is determined by the bulk properties, and one must improve the quality of the intrinsic layers of the top cell in order to obtain superior performance.

Since the first report[11] of improvement of stabilized performance of a-Si alloy films prepared with hydrogen dilution, there have been many studies to understand the role of hydrogen both in the plasma and in the material. Hydrogen dilution is known[12,13] to improve the material quality of a-Si:H by controlling the growth kinetics. With increasing hydrogen coverage, the surface mobility of the impinging species on the substrate increases, which should lead to a denser material with less microvoids. Because microvoids have been shown[14] to deteriorate device performance both in the initial and in the light-soaked stage, we decided to use hydrogen dilution for improving the performance of the top cell.

The initial J-V characteristic of a top cell using 2-3 times higher hydrogen dilution and 50-100° C lower substrate temperature than standard conditions[8] for the deposition of the intrinsic layer is shown in Fig. 7. As in the previous case, this device was deposited on a stainless steel substrate with no back reflector. A short-circuit current density (J_{sc}) of 7.4 mA/cm^2 is well suited for the top cell of a triple structure. We believe that the values of V_{oc} = 1.023 volts and fill factor (FF) = 0.773 are the highest reported to date for a-Si:H or a-SiC:H top cells.

We have also studied the stability of an "improved" top cell (B) and compared it with the "standard" top cell (A).[15] In Fig. 8 we plot the efficiency versus light-soaking time for the two samples. The initial and degraded J-V parameters are summarized in Table 1. It is noted that sample B not only exhibits higher initial efficiency but also better stability. In fact, the stabilized V_{oc} (0.98 V) and fill factor (0.71) represent the highest saturated values reported to date for a top cell.

It is interesting to note from Table 1 that sample B exhibits higher initial V_{oc} than sample A. To understand this V_{oc} difference, we made two thicker (intrinsic layer thickness ~ 4000 Å) cells using identical conditions as in samples A and B. We find, by measuring quantum efficiency and reflection of the solar cells and employing an optical model,[1] that the sample with higher hydrogen dilution and lower substrate temperature has a wider bandgap (1.81 eV) than the standard sample (1.74 eV). This explains the higher V_{oc} for sample B. Measurements of primary photocurrent reveal that the wider bandgap sample has similar Urbach tail but lower subgap absorption, suggesting a higher quality material.

From the above results, one can conclude that by using higher hydrogen dilution and optimized deposition conditions, one can obtain better stabilized performance for the top cell of a triple-junction structure. It should be pointed out that the same approach has been applied to the middle and bottom cells and preliminary data show improved performance. It is therefore anticipated that both the initial and stabilized performance of triple-junction devices will also improve accordingly.

Component Cell Optimization

In order to obtain improved performance of both double- and triple-junction modules, we have made component cells for the two cases and have studied their performance both in initial and light-soaked conditions. In our study, a-Si alloy was used for the top cells, and the bottom cells used amorphous silicon germanium (a-SiGe) alloy. For middle cells, both a-Si and a-SiGe alloys were used. The thicknesses of the cells were chosen so as to provide short-circuit current density as appropriate for the multijunction structure. The top and middle cells were deposited on textured substrate without any back reflector, since in the multijunction configuration these cells do not see much reflected light. The bottom cells were deposited on our conventional silver/zinc oxide (Ag/ZnO) textured back reflector.

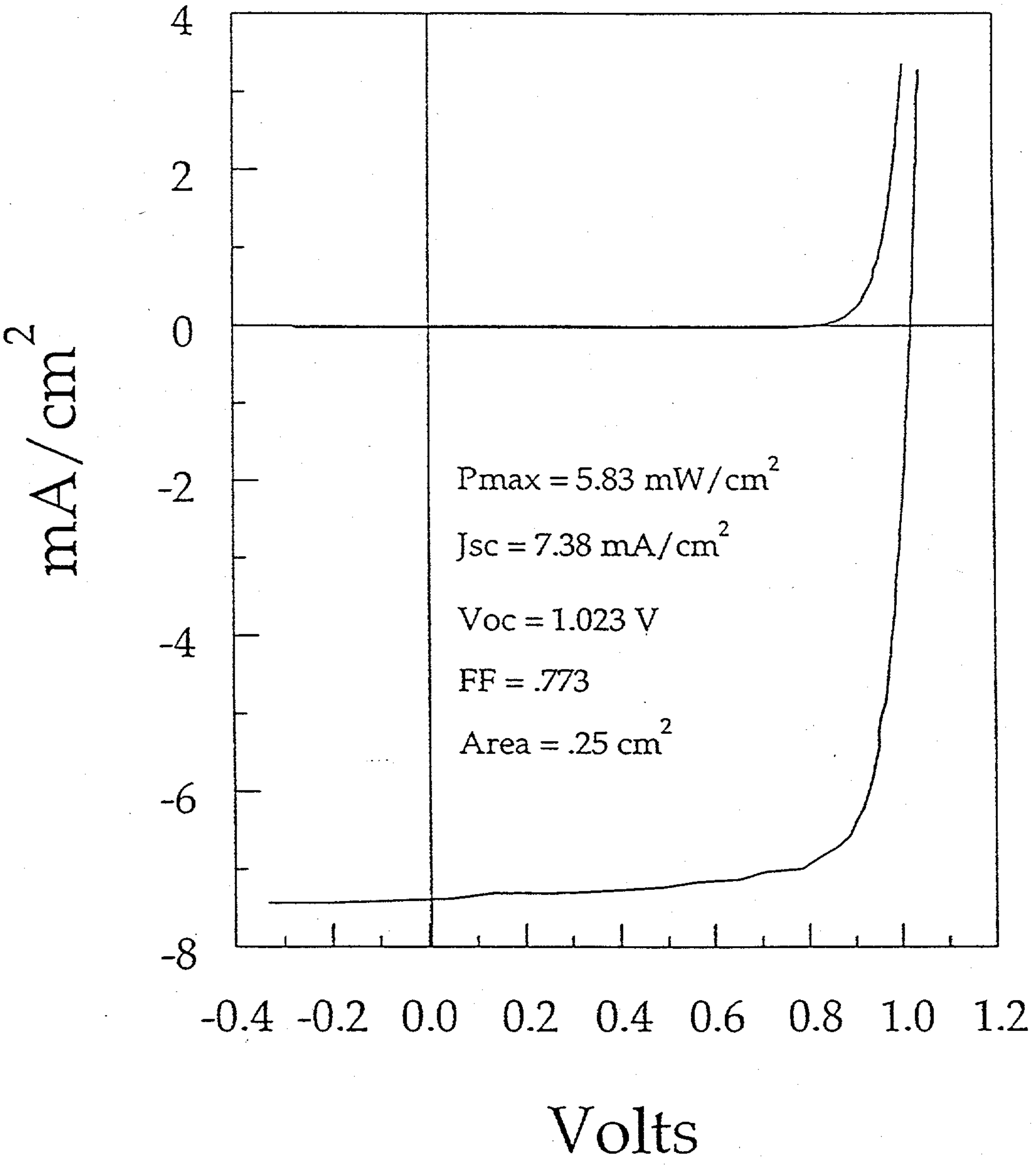

Figure 7. Initial J-V characteristic of the "improved" top cell.

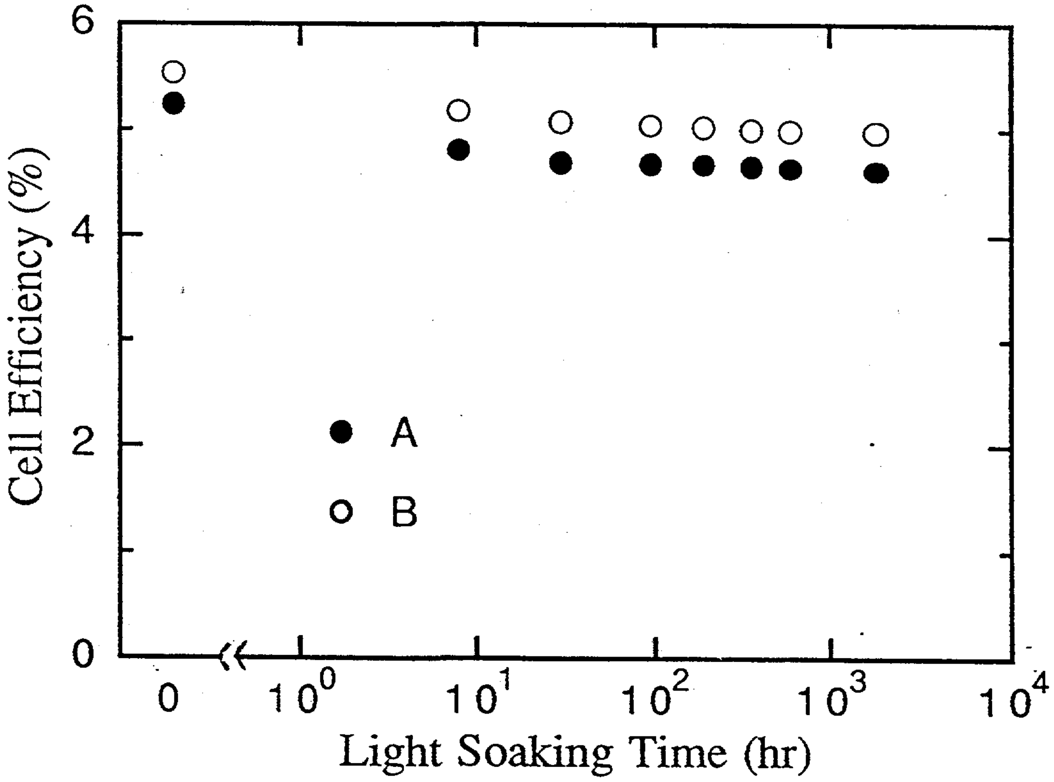

Figure 8. Light-induced degradation of "standard" (A) and "improved" (B) top cells.

Typical initial performances for state-of-the-art component cells for the triple-junction structure are shown in Table 3.[6] Also shown are the values after filtered one-sun (metal-arc lamp), 50 °C, 600 h light soaking. In this experiment, component cells were degraded under open-circuit condition at 50 °C for 600 h and measured at 25 °C. The top cell was degraded under one sun and measured under AM1.5 illumination; the middle cell was degraded under one sun with a 530 nm cut-on filter and measured under AM1.5 illumination with the same filter; the bottom cell was degraded under one sun with a 630 nm cut-on filter and measured under AM1.5 illumination with the same filter. We notice a degradation of 10% to 20% after light soaking. We should mention that one can improve the initial performance by making the component cells thicker, but this results in larger degradation and lower light-degraded efficiency.

We note that the component cells degrade between 9% to 18%. Similar studies[6] done on component cells for double-junction structure show a top cell degradation of 12% and a bottom cell degradation of 18%. However, the top cell of the triple-junction structure degrades by only 9% as compared to 12% for that of the double-junction structure. If one designs the multijunction structure in a way so as to make the operation limited by the top cell current, one would expect to see a lower degradation in triple-junction cells than that in double-junction ones.

As mentioned earlier, top cell in our structure does not use any carbon. By using hydrogen dilution to improve the quality of the i-layer and incorporating high conductivity microcrystalline p-layer[16] to improve built-in potential, we have obtained for the top cell an initial open-circuit voltage (V_{oc}) of 1.023 V, a fill factor (FF) of 0.77 and a short-circuit current density (J_{sc}) of 7.4 mA/cm^2. This is the best performance of the top cell as reported in the literature.

We should also mention that all the component cells in this study show true saturation in efficiency after prolonged light exposure. A typical example for the top and the bottom cell is shown in Fig. 9. The degradation is much lower than those obtained under intense light illumination, demonstrating the importance of thermal annealing of defects under normal operating conditions.

Microvoids and a-SiGe Alloy Cell Performance

We have previously reported[14] a correlation between microvoids and cell performance in a-Si alloys. It has been recently reported[17] that there is a sharp increase in the microvoid density of a-SiGe alloys as the Ge content increases beyond 20%. In order to determine if the observed poorer quality of a-SiGe alloys is related to this poorer microstructure, we have prepared a systematic set of samples of various Ge contents for small-angle X-ray scattering (SAXS) studies and solar cell characterization.[18] The results are reported here.

Details of SAXS measurements and interpretation have been published earlier.[19] In Table 4, we show the properties of a-SiGe alloy films with different Ge content (X) and optical gap (E_0) prepared at different substrate temperatures (T_s). Q_0 is a measure of the microvoid density as obtained from the SAXS data.[14] Q_{45} is the corresponding value with the sample tilted 45° with respect to the incident beam.

A significant increase in SAXS is seen as the Ge content increases beyond 20%. Below 20%, the Q_0 values are comparable to those for device-quality a-Si alloy. From measurements made with samples tilted with respect to the incident beam, the increase in scattering beyond 20% Ge content is attributed to the appearance of elongated low density regions in the film, modeled as ellipsoidal microvoids, which may be related to columnar growth. From Table 4, we also find that for the high Ge content samples, SAXS increases as the substrate temperature increases from 350 to 400 °C. This is contrary to what one observes in a-Si alloys.

Table 3. **Present Status at USSC of Typical Initial and Degraded Cell Parameters for Component Cells Degraded and Measured under Conditions Described in the Text.** The high- and the mid-bandgap cells use Cr as back reflector. Use of Ag/ZnO as back reflectors for these cells increases J_{sc} by 30% to 40%.

			J_{sc} (mA/ cm^2)	V_{oc} (V)	FF	P_{max} (mW/ cm^2)
a-Si	high-bandgap cell	initial	7.3	1.01	0.75	5.53
		degraded	7.2	0.98	0.71	5.01
		degradation (%)	1.4	3.0	5.3	9.4
a-Si	mid-bandgap cell	initial	6.44	0.90	0.70	4.02
		degraded	6.22	0.87	0.61	3.29
		degradation (%)	3.4	3.3	12.9	18.2
a-SiGe	mid-bandgap cell	initial	7.02	0.77	0.65	3.51
		degraded	6.85	0.74	0.57	2.89
		degradation (%)	2.4	3.9	12.3	17.7
a-SiGe	low-bandgap cell	initial	7.8	0.67	0.64	3.34
		degraded	7.7	0.65	0.56	2.80
		degradation (%)	1.3	3.0	12.5	16.2

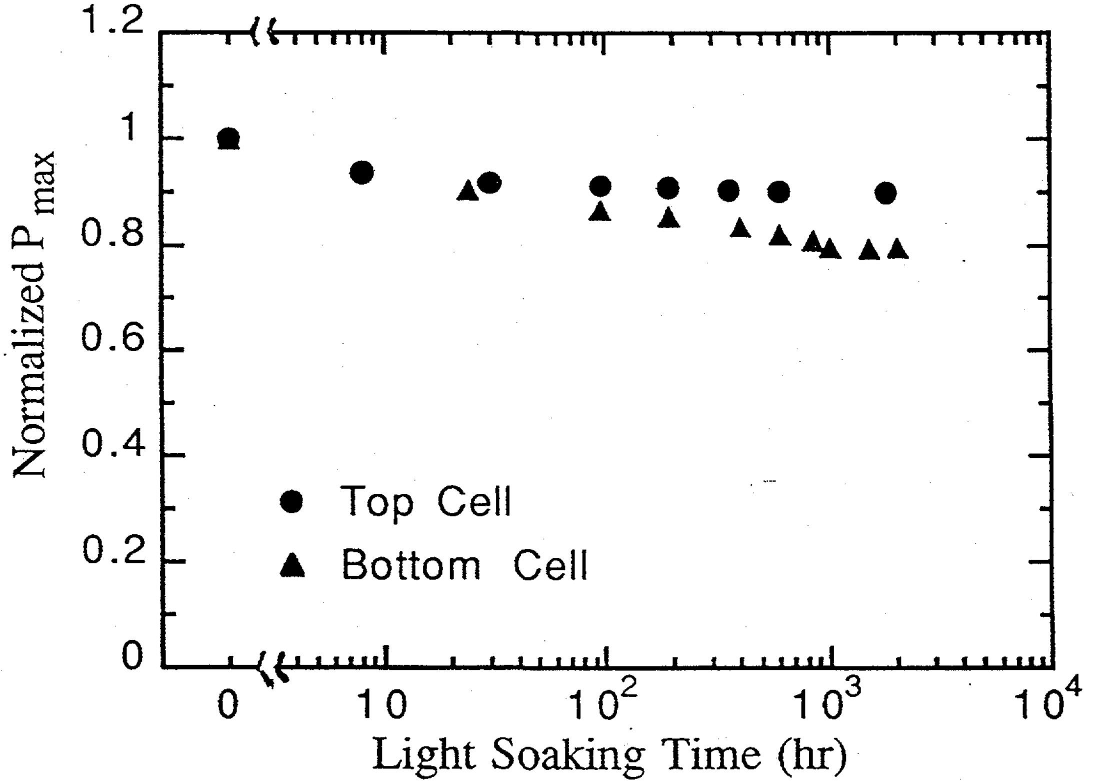

Figure 9. Saturation in light-induced degradation of component cells.

Table 4. Measured Properties for the a-$Si_{1-x}Ge_x$:H Films.

Sample	X	E_o (eV)	T_s (°C)	Q_0 (10^{-6} nm^{-2})	Q_0/ Q_{45}	Laue Monotonic Intensity (10^{-7} nm^{-2})	Film Density (g/cc)	Density Deficiency (%)
4810	0	1.72	300	1.0	-	1.0	-	-
5525	0.09	-	350	1.3	1.0	2.6	2.54	3.4
5526	0.09	-	250	0.4	0.9	2.8	2.61	0.7
4838	0.19	1.55	350	1.1	1.1	3.2	2.98	-0.7
4835	0.31	1.50	350	2.4	1.3	5.2	3.26	2.7
4837	0.41	1.41	350	5.9	2.5	4.6	3.50	4.4
5445	0.44	-	400	9.2	5.3	3.7	3.60	4.0

In Figs. 10 and 11, we show the initial and light-degraded properties of the a-SiGe:H solar cells with different germanium contents. Included for comparison are the values of Q_0 from the SAXS. In an attempt to compare films with similar bonded hydrogen contents, we include in the figures only values for films prepared at substrate temperatures of 350 °C except for the a-Si:H film which was deposited at 300 °C. Several points emerge. There is a decrease in V_{oc} and a corresponding increase in J_{sc} as the germanium content increases. This is expected since the optical gap decreases with increasing Ge content. All of the initial photovoltaic parameters shown appear to change smoothly with X with no indication of a sharp change above $X = 0.2$ where the Q_0 values rise significantly. This indicates that other changes are taking place in the material when Ge is added which are not detected by SAXS. It has been demonstrated that addition of Ge increases the width of the conduction band tail, presumably caused by alloy disorder.[19] This would, of course, not be detected by SAXS. Increase of isolated dangling bond density caused by introduction of germanium would cause a reduction in fill factor but will not be detected by SAXS. Moreover, since the sensitivity in the SAXS measurement for the film thickness used here (~ 1 μm) is on the order of $\pm 0.5 \times 10^{-6}$ nm^{-2} and the magnitude of SAXS signal measured for the $X = 0.19$ sample is only 1.1×10^{-6} nm^{-2}, we cannot rule out a systematic decrease in SAXS as the Ge content is lowered below $X = 0.2$, which cannot be detected with the sensitivity realized in these measurements.

The lack of any definite enhanced deteriorations in the initial photovoltaic properties when the SAXS increases dramatically at X around 0.3-0.4 suggests that, for at least this set of films, the role of the SAXS detected microstructure is perhaps relatively minor. Lack of added information on these samples including bonded hydrogen contents, a complete list of optical gaps and defect densities impedes us from making a more definitive statement. If the columnar-like microstructure detected by SAXS does not affect the initial solar cell properties, two points of interest can be made. First, it has been shown that a sharp decrease in the photoconductivity-to-dark conductivity ratio and increase in the sub-bandgap absorption detected by photothermal deflection spectroscopy accompany the sudden increase in Q_0 at around $X = 0.2$-0.3,[17] suggesting that the appearance of columnar-like microstructure can alter the photoelectronic properties. This result would seem to contradict the lack of correlation of Q_0 with the a-SiGe:H solar cell properties. However, the photoconductivity measurements were done with the electrodes in the co-planar configuration, in contrast to the solar cell sandwich design. One could envision that in the solar cell a majority of the conduction of electrons and holes takes place in the high density, less defective column regions without the carriers passing through the low density regions which comprise a relatively small volume fraction of the material. In contrast, for the carriers to reach the co-planar electrodes, they must move parallel to the film surface and likely pass through low density material lying between the columns. Second, while no definite correlations can be made between the SAXS and the solar cell properties for a-SiGe:H, a clear dependence of the initial solar cell efficiency on the SAXS-detected microstructure in a-Si:H was noted.[14] But the nature of the scatterers in these two cases is quite different. In contrast to anisotropic, columnar-like microstructure in the alloys, the scatters detected in the a-Si:H with the poor cell properties were spherical and/or randomly oriented and smaller (~ 1 nm) than those which appear in the alloys. Therefore, the effect of microstructure on the solar cell properties may depend on details such as void size, shape and orientation.

Finally, note that the fractional degradation characteristics shown in Fig. 11 suggest larger amounts of degradation for $X \geq 0.2$ (except V_{oc}), and this may correlate with the SAXS-detected microstructure. However, more data is needed before a definite conclusion can be reached, and detailed discussion is warranted.

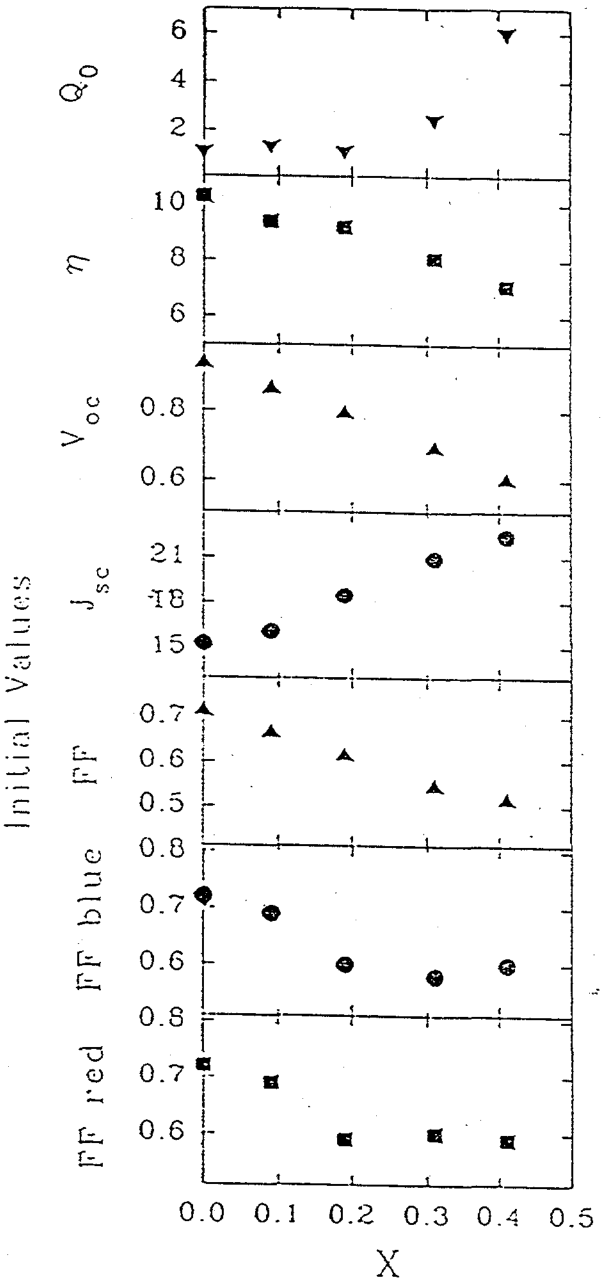

Figure 10. **Initial solar cell performance and microvoid density as function of germanium content.**

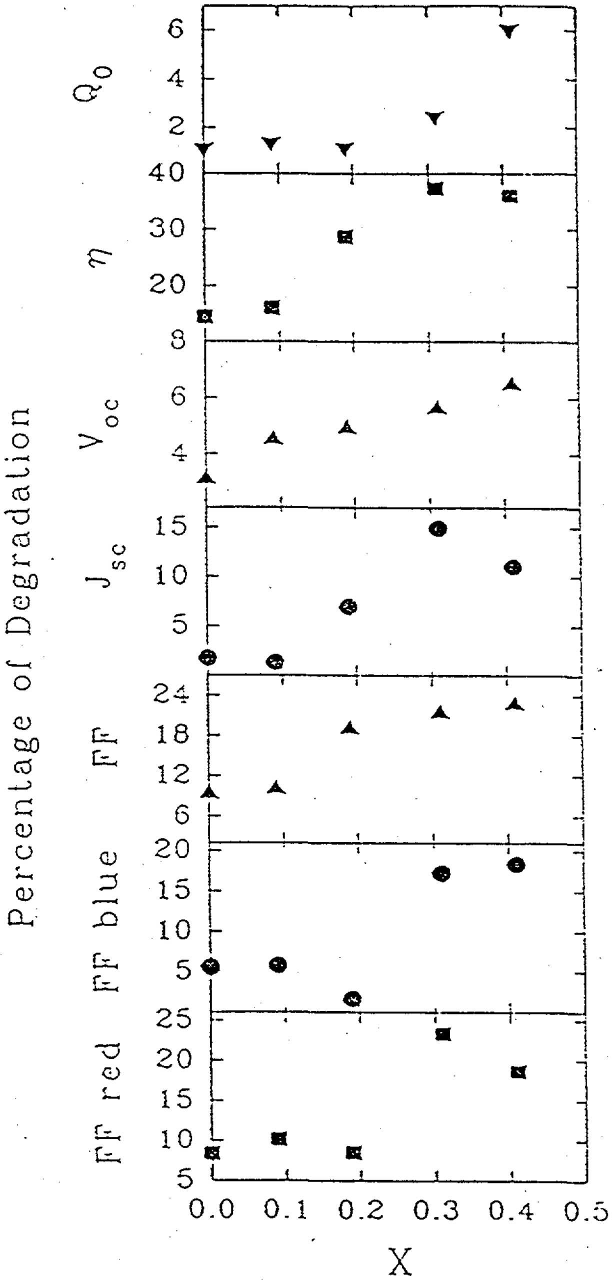

Figure 11. Fractional degradation of solar cell performance and microvoid density as a function of germanium content.

Cell Stability Under Different Light Spectrum

We have been carrying out light-induced degradation studies using a metal arc lamp which has a different spectrum from global AM1.5 (Fig. 12). In order to ascertain the effect of this difference in spectrum on cell stability, we have carried out degradation studies on both double- and triple-junction cells using the metal arc source and also a global AM1.5 simulator. The samples used are small-area cells obtained in the same deposition run. The results for double- and triple-junction cells are shown in Figs. 13 and 14, respectively. We find virtually no difference in the cell degradation using the two light sources. Light soaking under the metal arc lamp can therefore be used to ascertain the degradation under global AM1.5 condition.

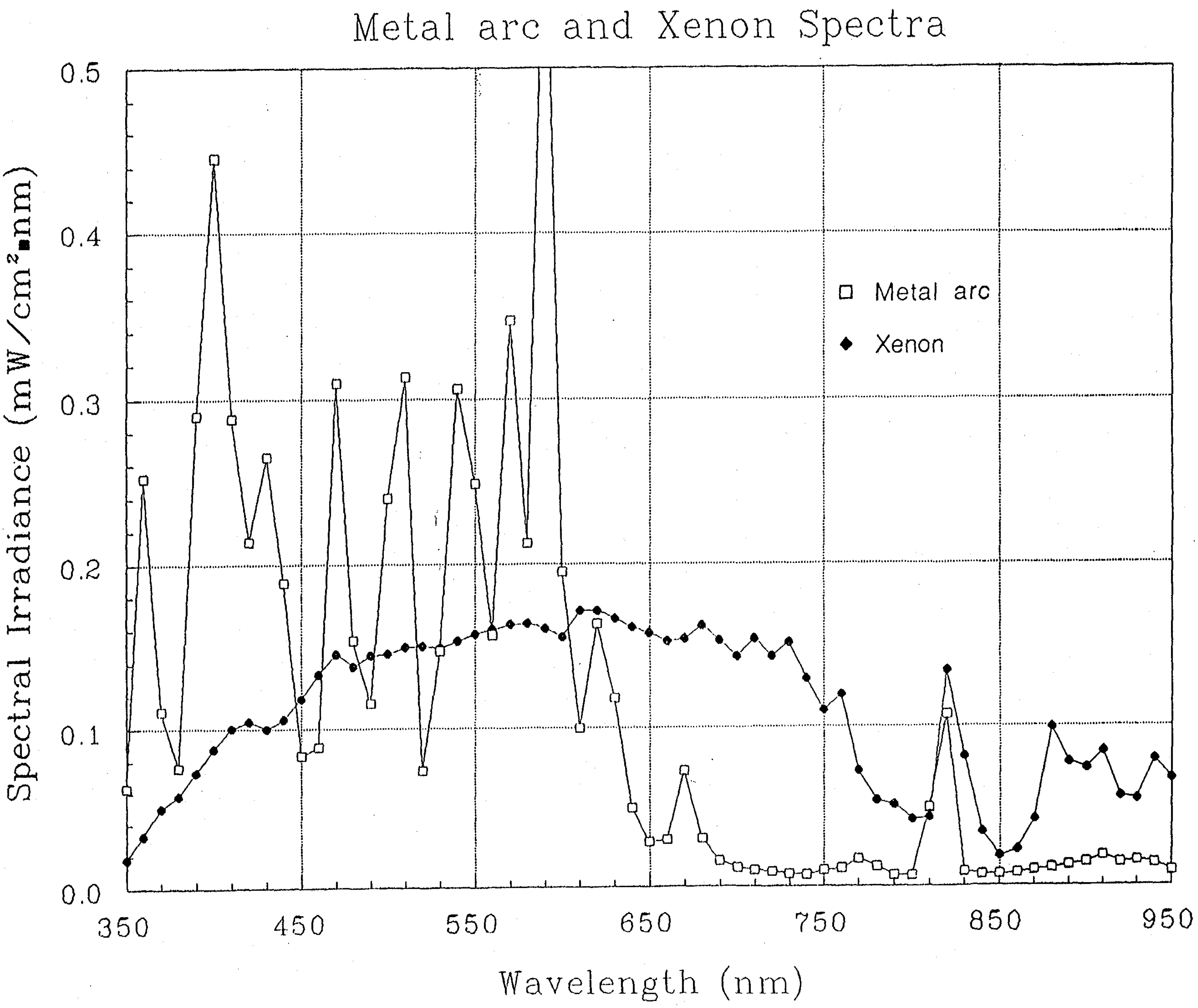

Figure 12. Spectrum of the metal arc lamp source and global AM1.5 simulator.

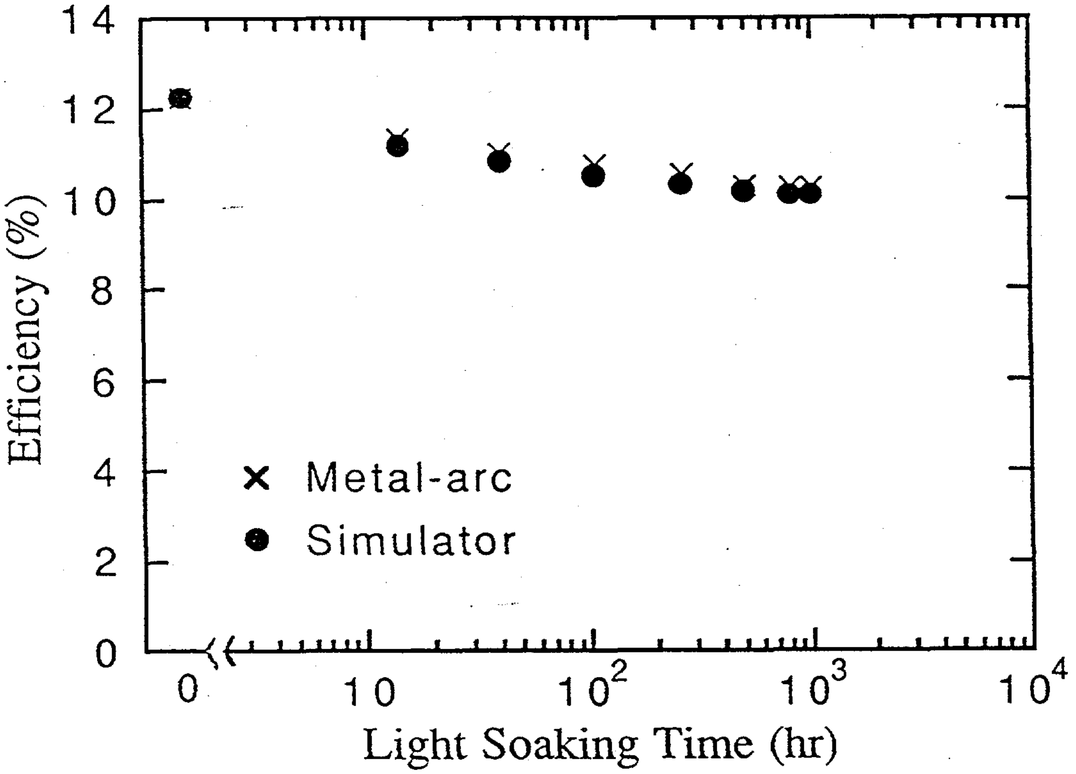

Figure 13. Degradation of double-junction cells after light soaking under the metal arc lamp and global AM1.5 simulator.

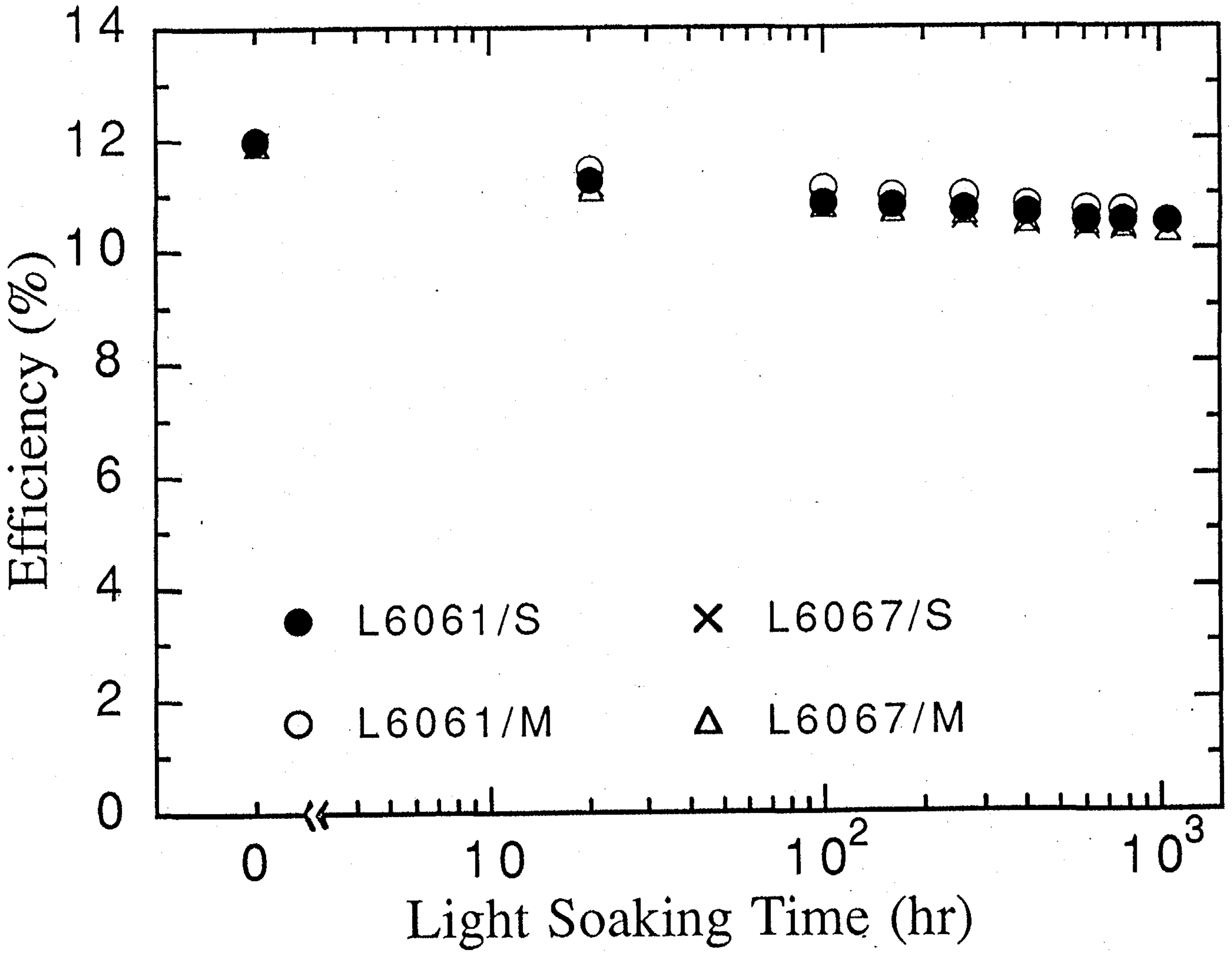

Figure 14. Degradation of triple-junction cells after light soaking under metal arc lamp (M) and global AM1.5 simulator (S).

Section 4

Large-area Deposition and Module Research

Introduction

Significant progress has been made on both module and device results since the end of Phase II. The 2B machine has been used to prepare cells for large-area (~ 900 cm^2) module fabrication. Both dual-bandgap, double-junction and triple-bandgap, triple-junction structures have been studied. The top cell in both cases consists of an a-Si:H i-layer, and the middle and bottom cells have a-SiGe:H alloy i-layers. The back reflector consists of a textured Ag/ZnO film on a stainless steel substrate.

The cell fabrication procedure consists of first preparing the back reflector using a sputter deposition technique. The coated area is greater than 900 cm^2. The n, i, p layers are then deposited in the 2B machine. This is followed by an antireflection coating of ITO and top grid contact. The module is fabricated by appropriate encapsulation using EVA and Tefzel.

In this report, the major emphasis is on double-junction modules. Initial module efficiency as high as 11.4% has been confirmed by NREL. The high efficiency has been attained as a result of careful and systematic analysis and optimization of component cells, "tunnel" junction between the top and bottom cells, and uniformity over an area of 900 cm^2.

Progress of March 1993 - November 1993

Device Results

The J-V characteristic and Q curve of a small-area ~ 0.25 cm^2 optimized double-junction cell are shown in Fig. 15. The efficiency is 12.77%, which is the highest obtained on a 2B machine-fabricated device. The values of J_{sc}, V_{oc}, and FF are 10.8 mA/cm^2, 1.691 V, and 0.699, respectively. The corresponding efficiency reported at the end of Phase II was 12.08%. The contributions to J_{sc} from the top and bottom cells (see Q curve of Fig. 15) are 10.59 and 10.9 mA/cm^2, respectively, which translates to a total current density of 21.49 mA/cm^2.

The J-V characteristic of the top cell of a triple made on a stainless steel substrate is shown in Fig. 16. The values of J_{sc}, V_{oc}, FF, and efficiency are 7.2 mA/cm^2, 0.984 V, 0.759, and 5.4%, respectively. The active area of the cell is 0.82 cm^2.

The J-V characteristic of a 0.82 cm^2 active area optimized triple-junction device is shown in Fig. 17. The efficiency is 12.47%. In comparison, the best corresponding efficiency reported at the end of Phase II was 11.15%. This result represents a significant improvement. The values of J_{sc}, V_{oc}, and FF for the device shown in Fig. 17 are 7.2 mA/cm^2, 2.466 V, and 0.702, respectively.

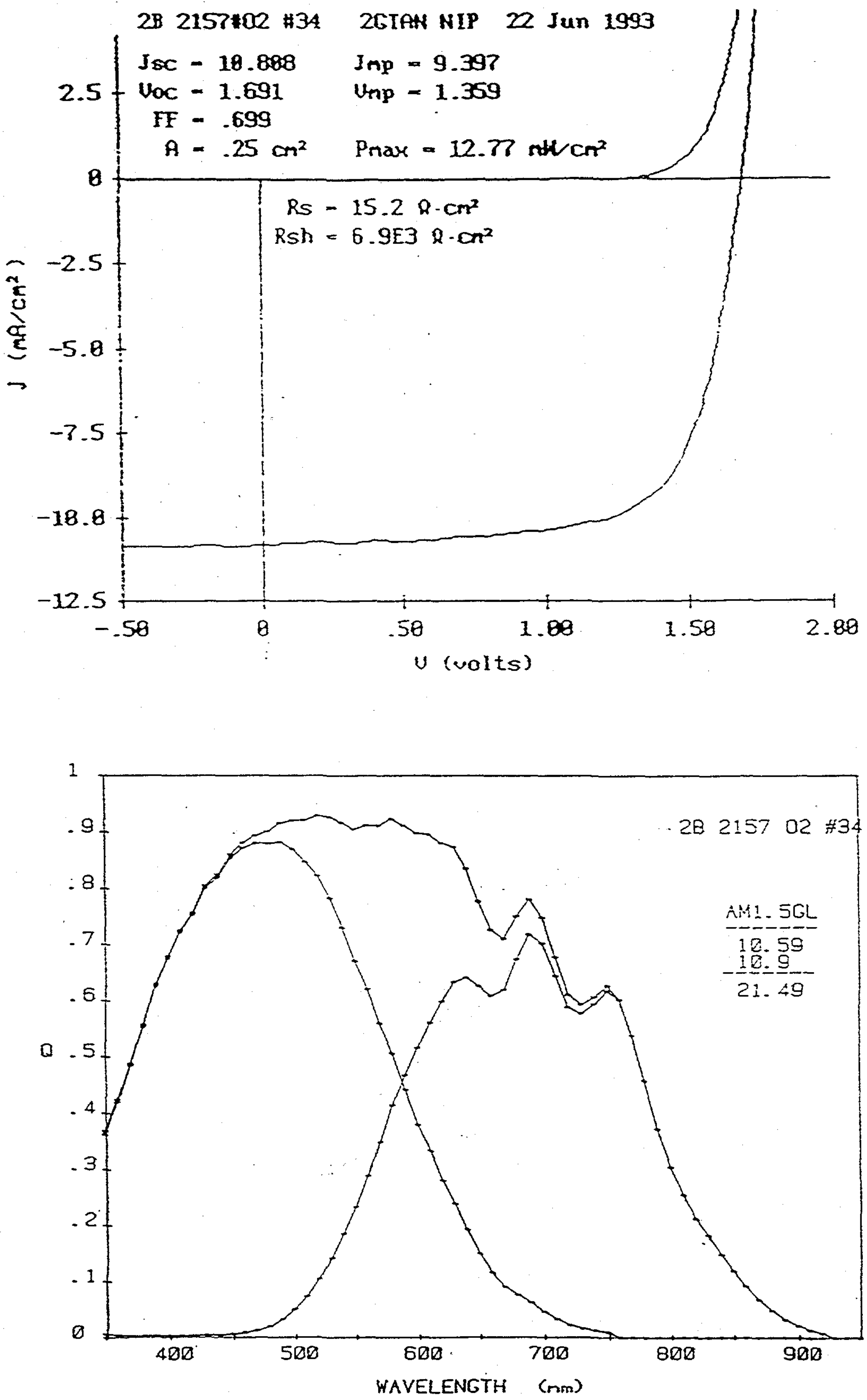

Figure 15. J-V characteristic and Q curve of a 0.25 cm^2 area double-junction cell.

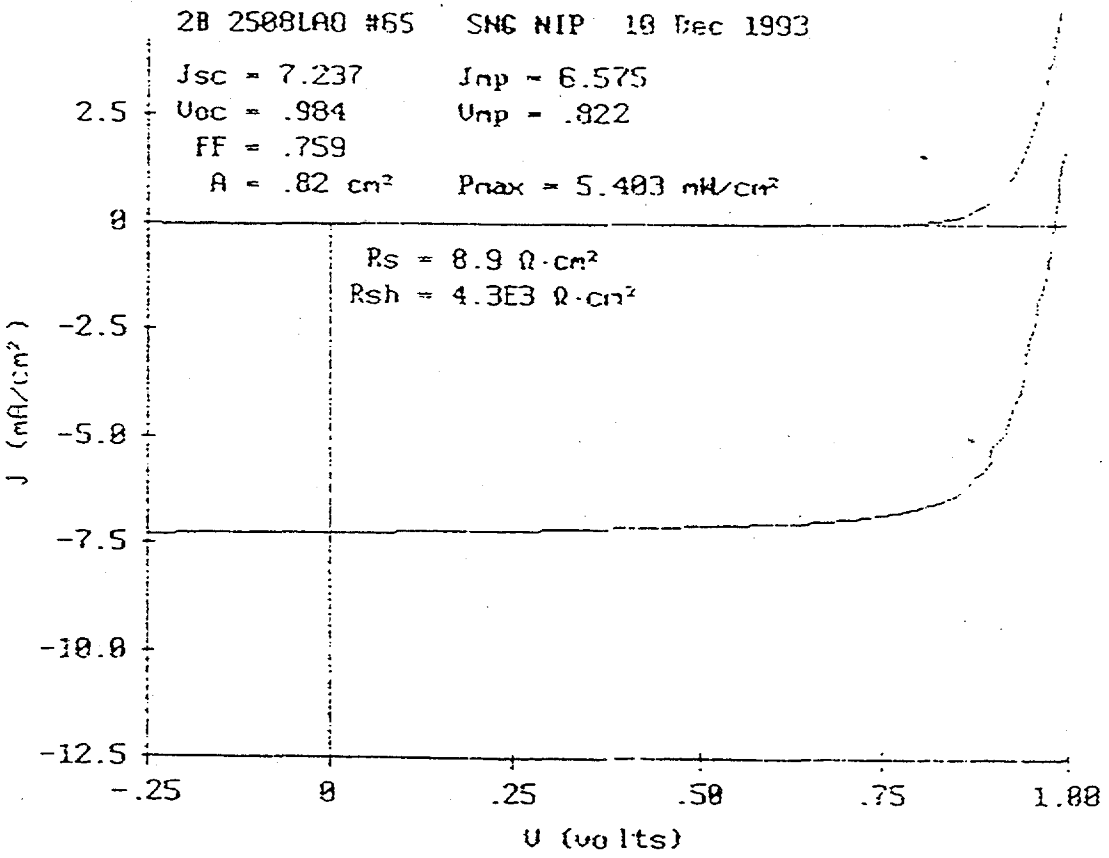

Figure 16. J-V characteristic of the top cell of a triple-junction cell on ss substrate.

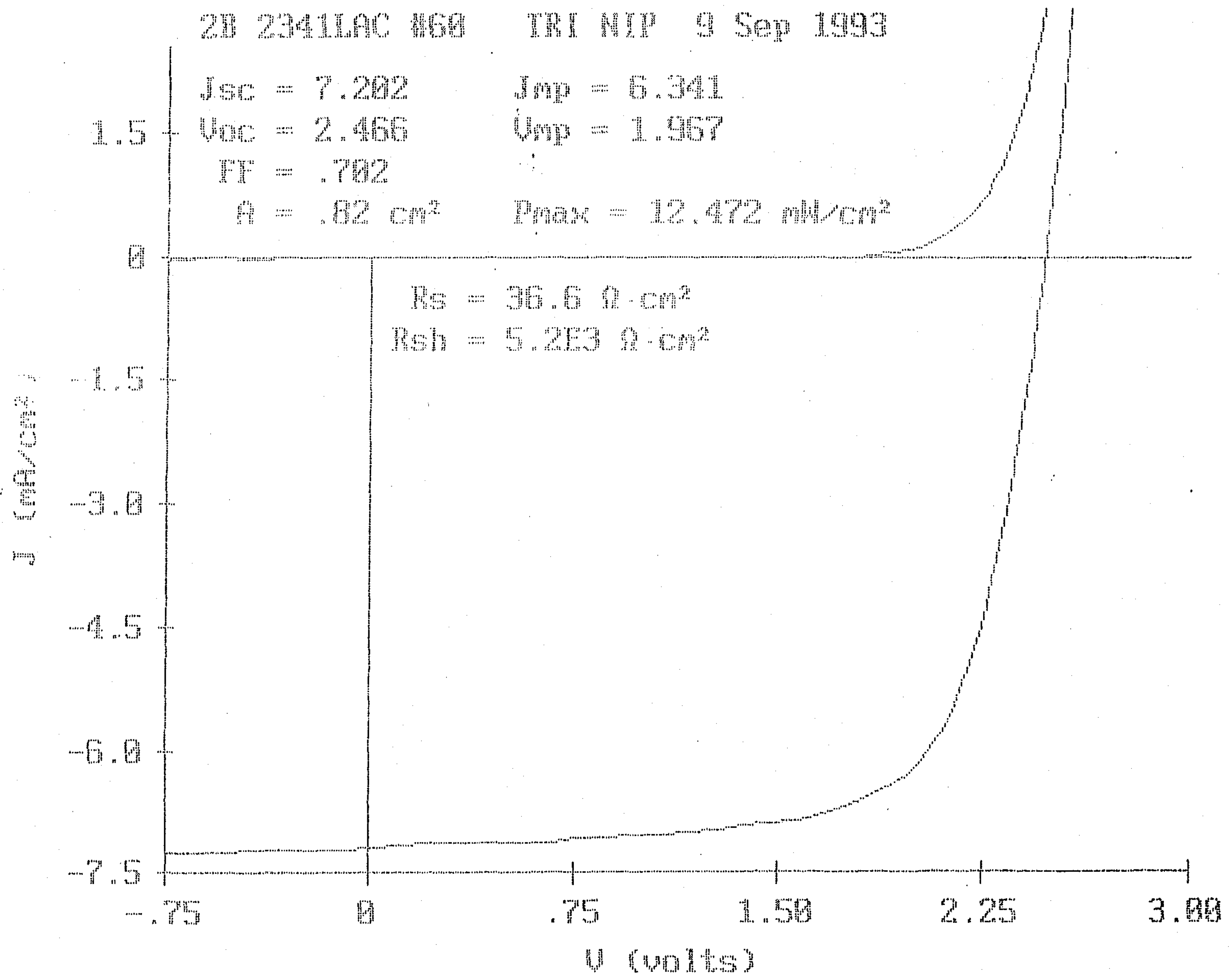

Figure 17. J-V characteristic of a 0.82 cm^2 area triple-junction cell.

Uniformity Studies

The uniformity studies have been carried out by delineating an array of 132 devices arranged in a matrix of 12 x 11 over the 900 cm^2 area and measuring the performance on all the cells. Equal value contour plots of V_{oc}, FF, J_{sc}, and efficiency of the top cell of a triple made on a stainless steel substrate are shown in Figs. 18-21, respectively. The corresponding contour plots of a triple-junction device are shown in Figs. 22-25. The efficiency contour plot of the triple (see Fig. 25) shows that the nonuniformity over the entire 900 cm^2 area is within 5% between the highest and lowest values. The contour plots for the double-junction cells and the component cells have been shown in the Phase II report.

Module Results

Four double-junction modules fabricated at USSC have been measured by NREL under both indoor and outdoor conditions. The results are summarized in Table 5. The highest values of indoor and outdoor initial efficiency obtained are 11.4% and 11.0%, respectively. These values correspond to a new world record for any thin-film module confirmed by NREL as regards initial efficiency measurements.

A few preliminary triple-junction modules have been fabricated. The efficiency is typically 10.5%-11.0%. Further optimization is expected to lead to higher efficiency.

The progress in module efficiency over the past two years is shown graphically in Fig. 26. All the data shown in the figure were obtained on double-junction modules. The graph shows a continuous improvement in module efficiency from 7.5%-8.1% in November 1991 to 10.7%-11.4% in July 1993.

Stability Studies

The double-junction modules have been subjected to indoor light soaking studies. The test was done under one sun, 50 °C at maximum power point loaded conditions. The efficiency of a module of initial efficiency 11.1% as a function of time is shown in Fig. 27. The stabilized value after 1000 hours of illumination is 9.5% which is the highest obtained on any a-Si module.

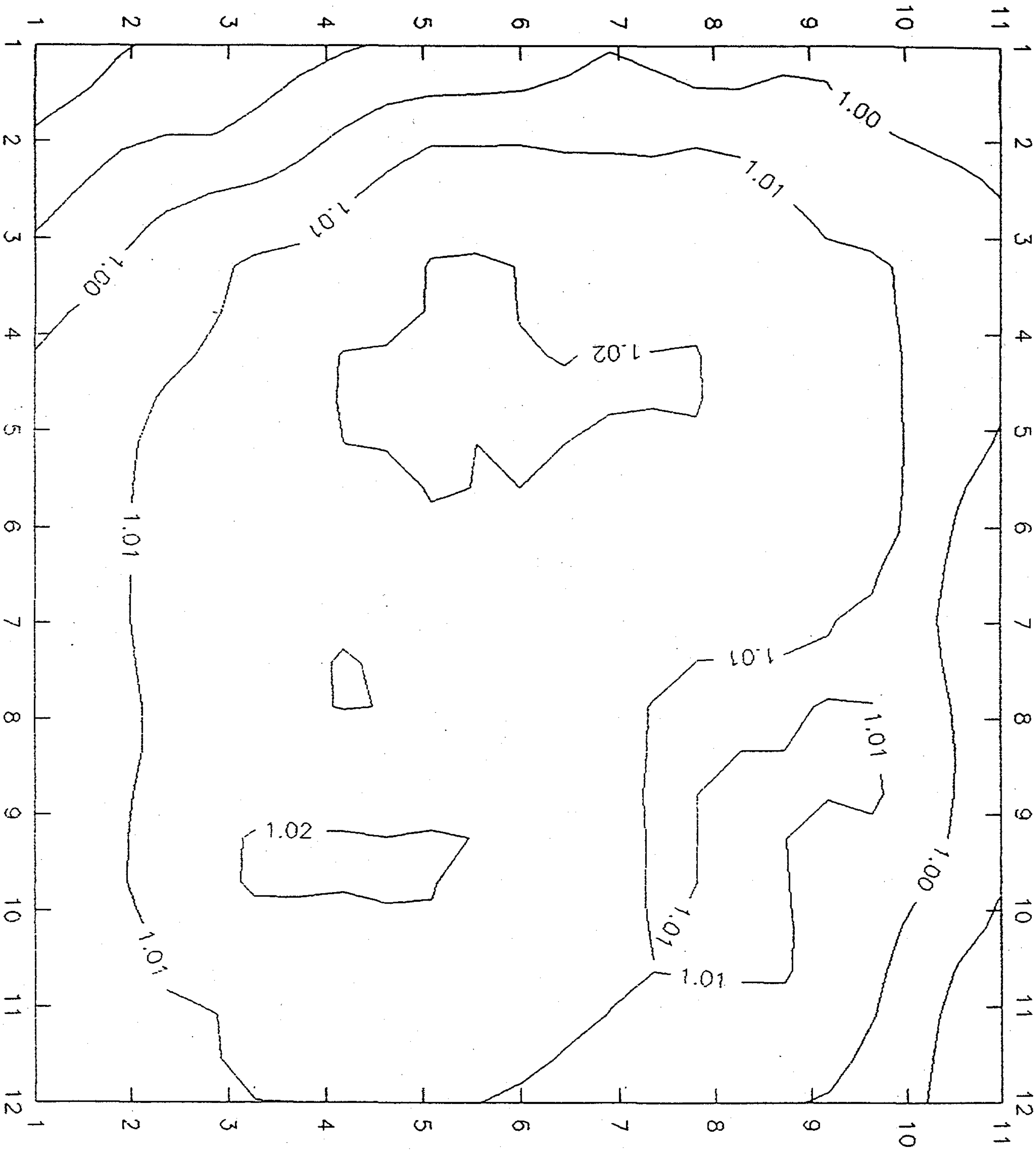

IIB 2403 Voc

Figure 18. V_{oc} contour plot of the top cell of a triple-junction cell over 1 ft x 1 ft area..

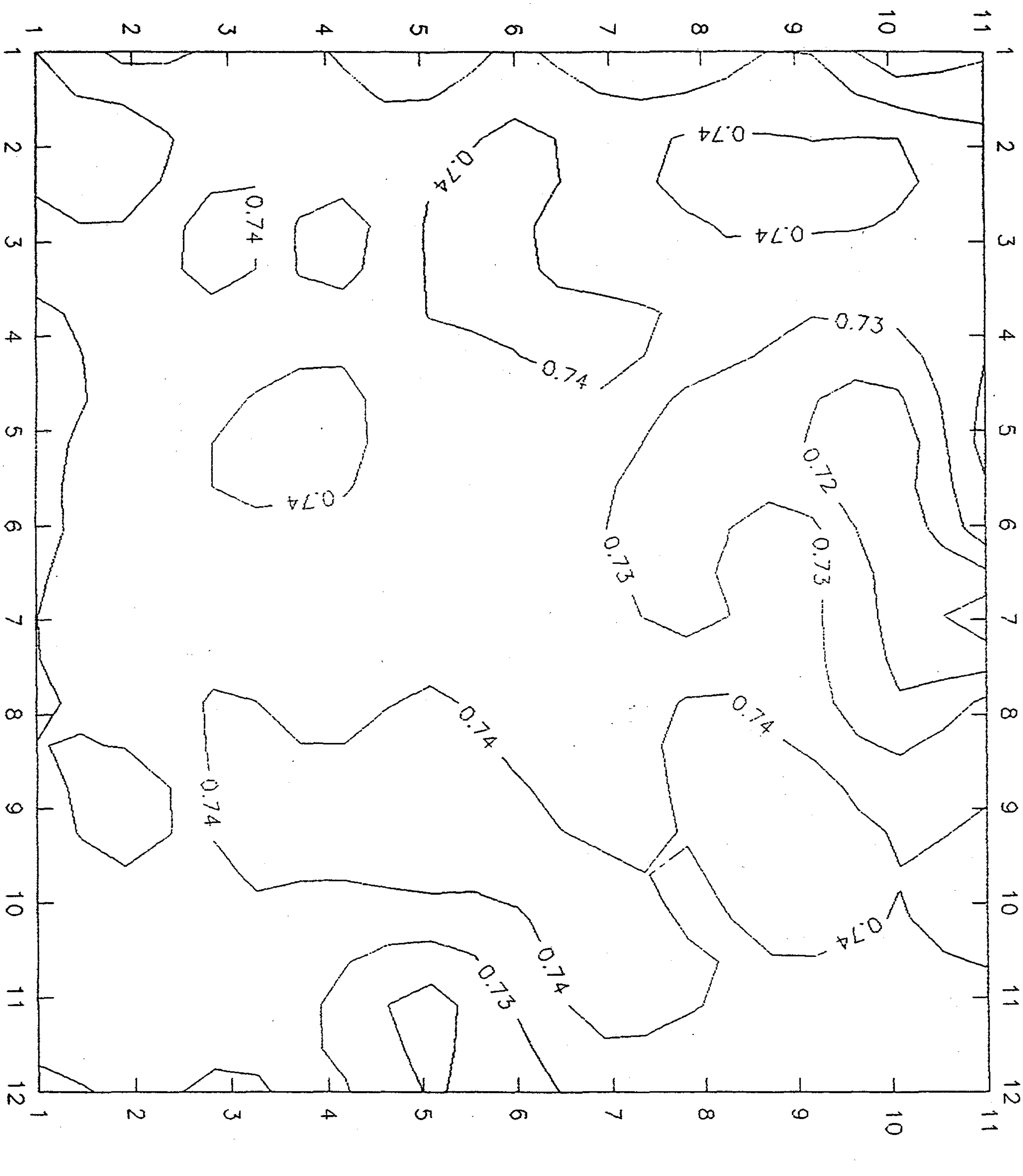

IIB 2403 FF

Figure 19. **FF contour plot of the top cell of a triple-junction cell over 1 ft x 1 ft area.**

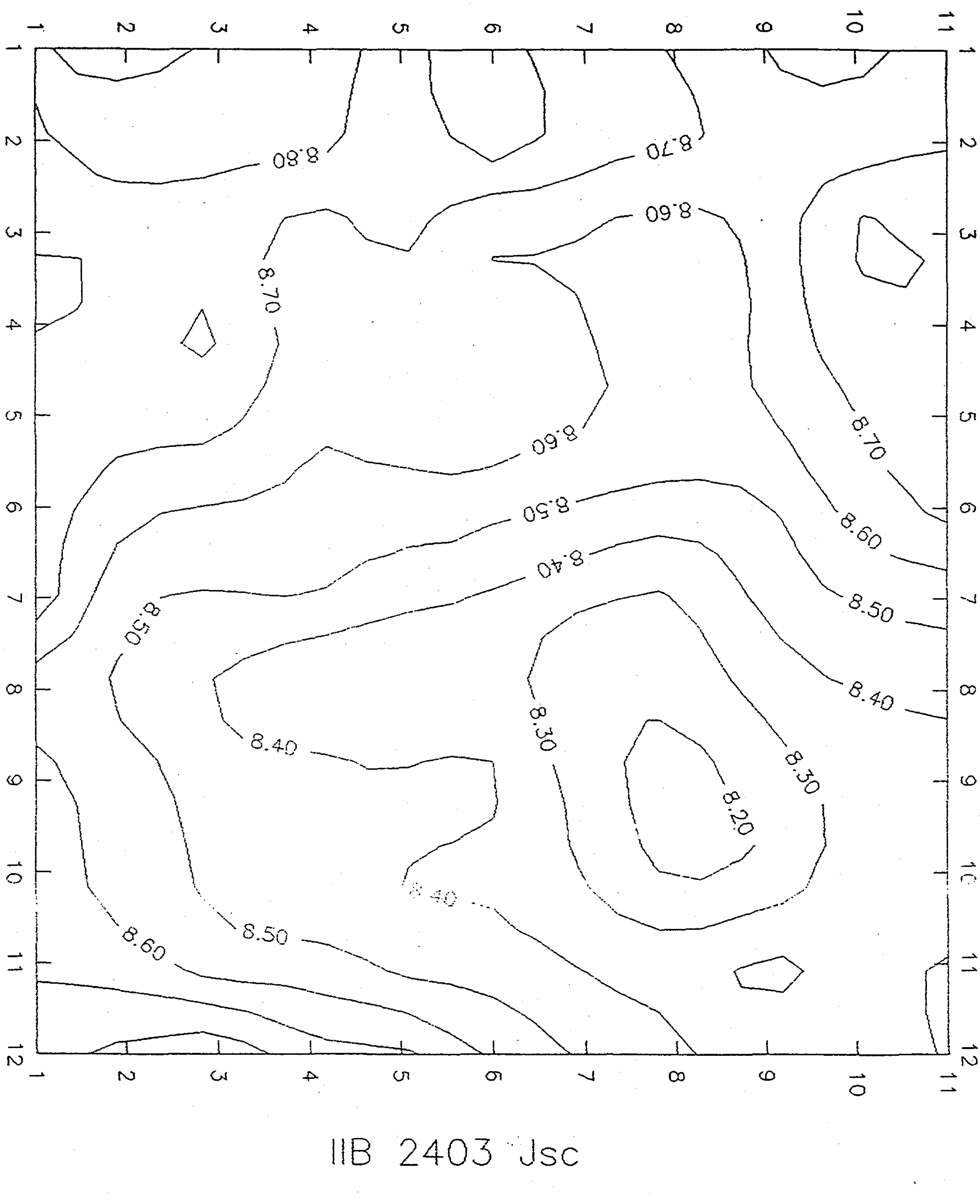

Figure 20. J_{sc} contour plot of the top cell of a triple-junction cell over 1 ft x 1 ft area.

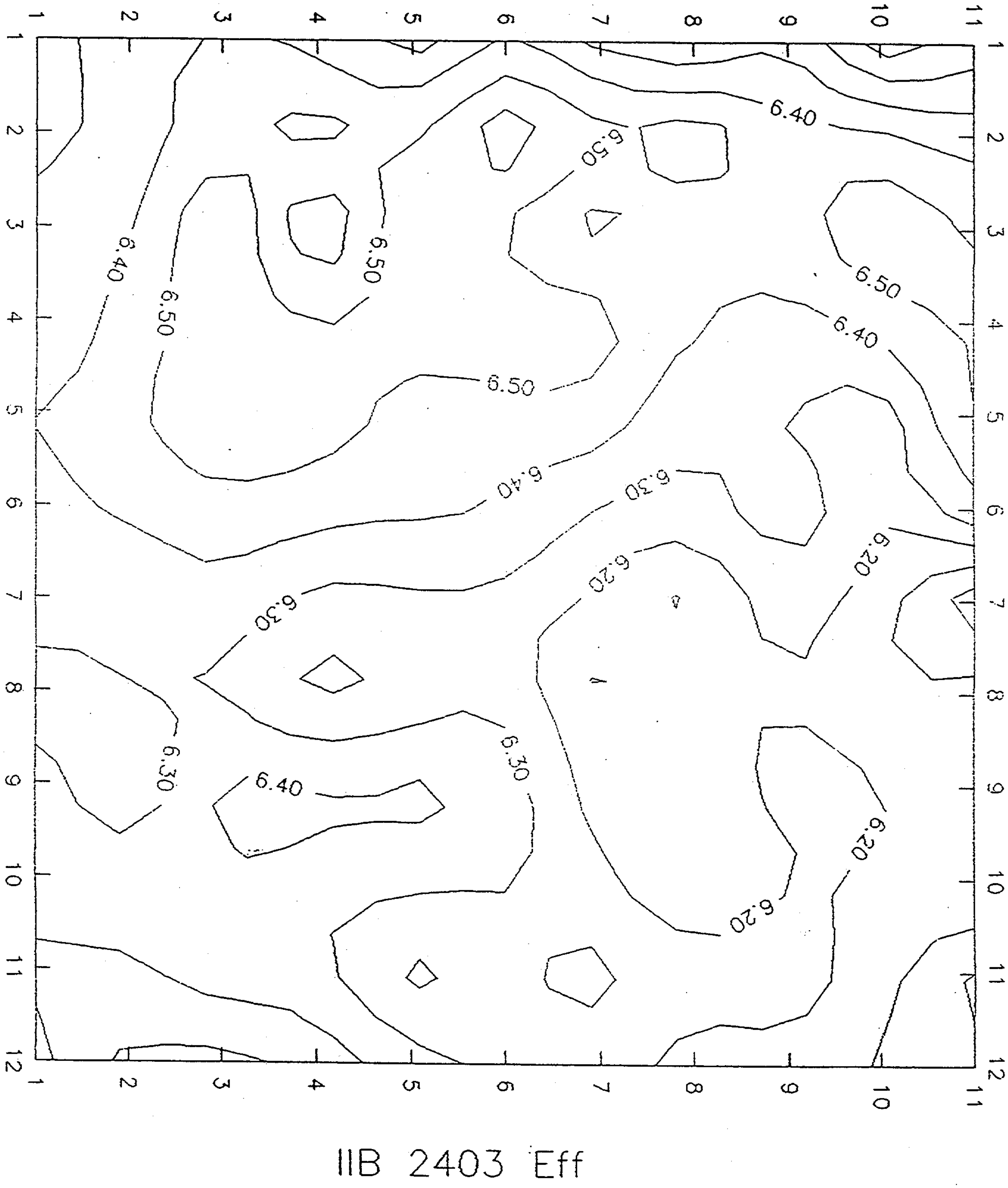

Figure 21. Efficiency contour plot of the top cell of a triple-junction cell over 1 ft x 1 ft area.

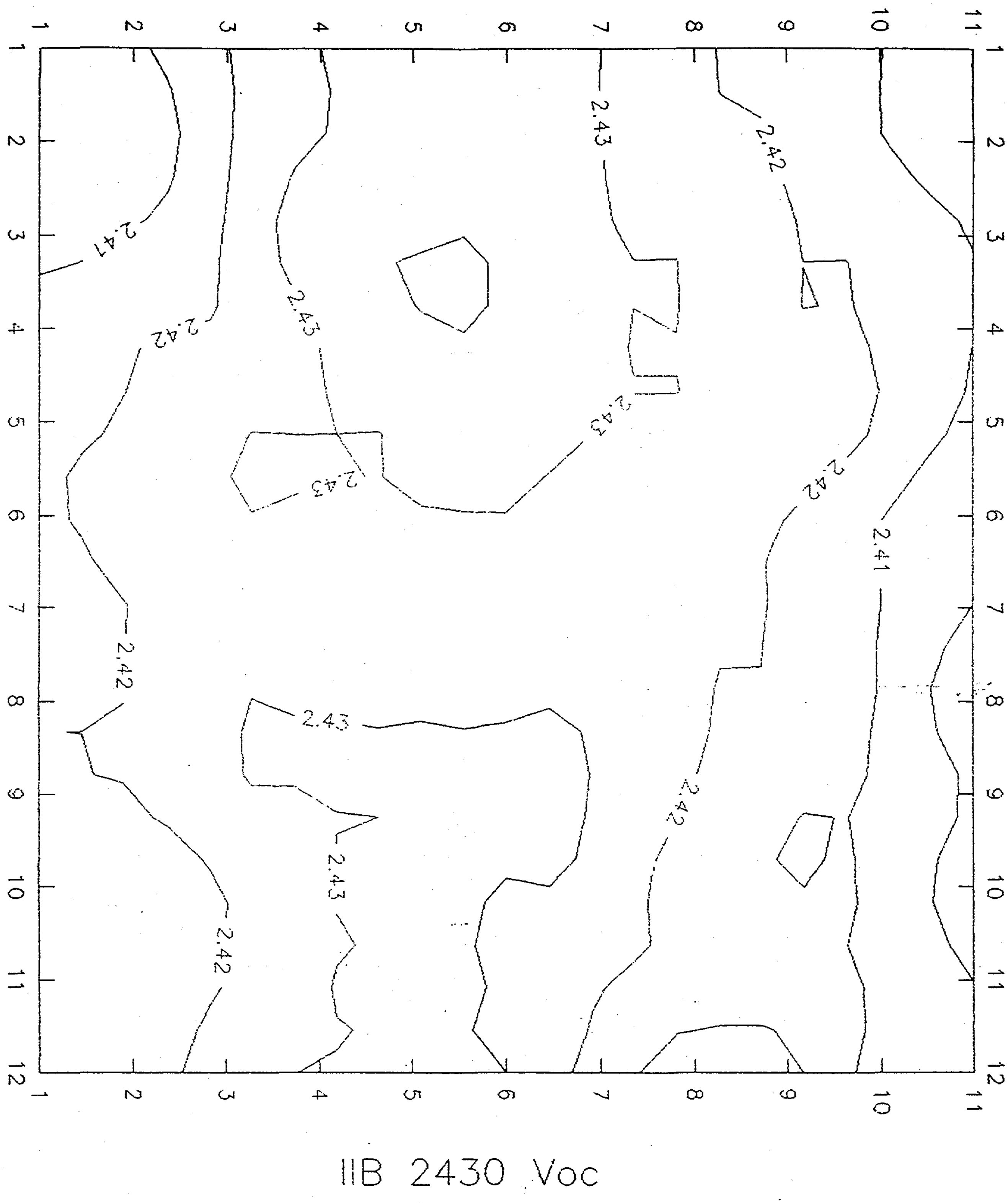

Figure 22. V_{oc} contour plot of a triple-junction cell over 1 ft x 1 ft area.

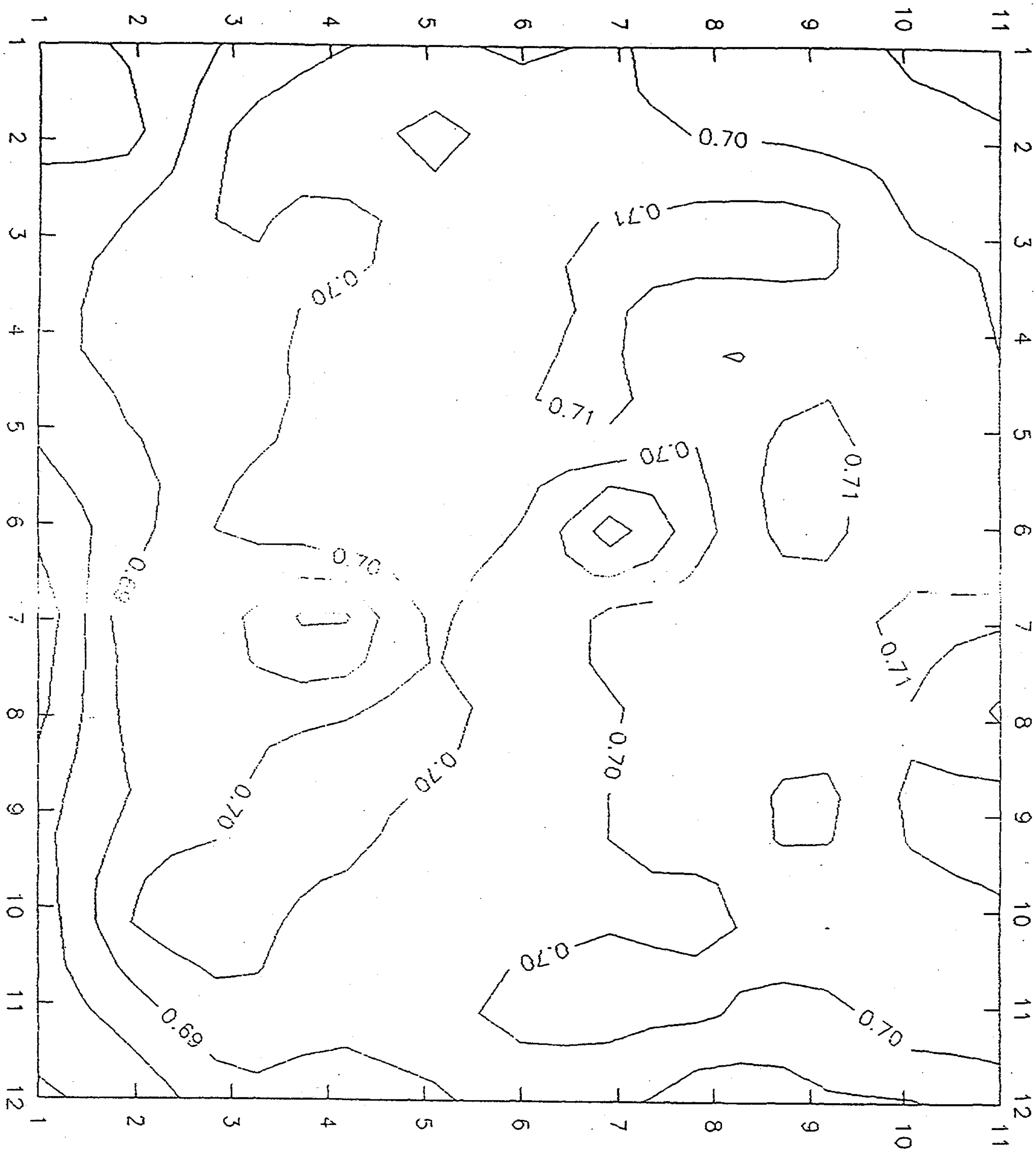

IIB 2430 FF

Figure 23. FF contour plot of a triple-junction cell over 1 ft x 1 ft area.

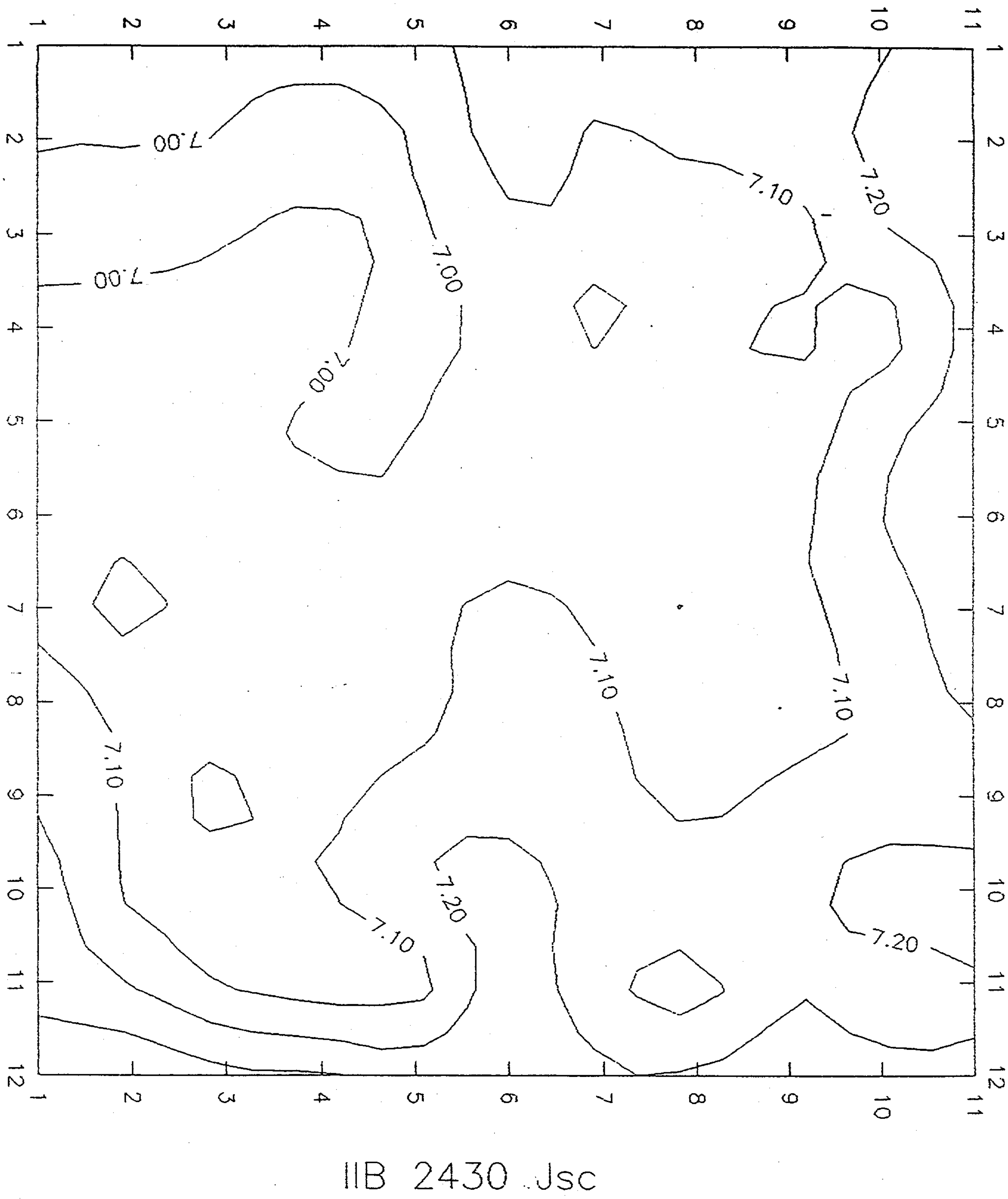

Figure 24. J_{sc} contour plot of a triple-junction cell over 1 ft x 1 ft area.

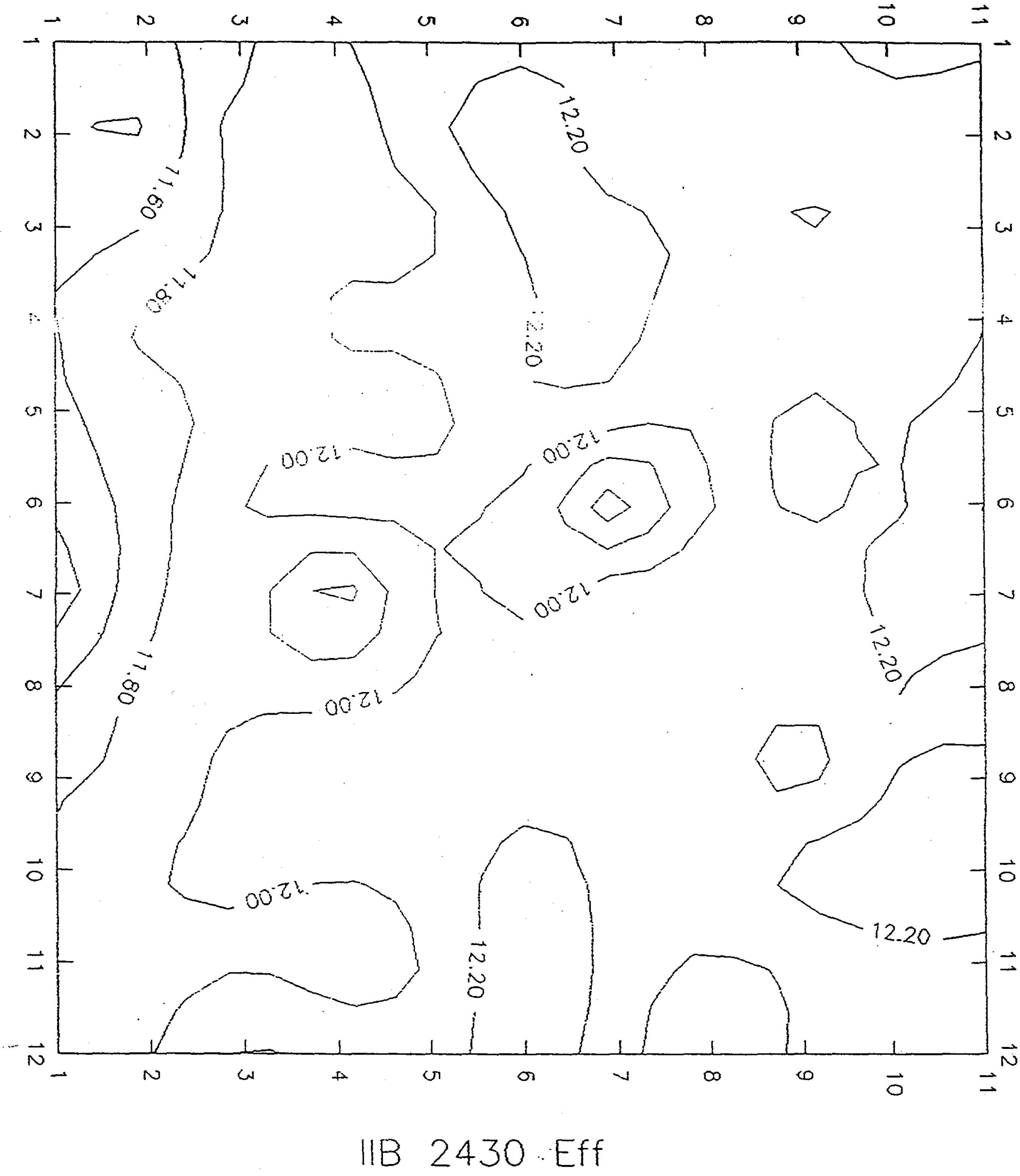

Figure 25. Efficiency contour plot of a triple-junction cell over 1 ft x 1 ft area.

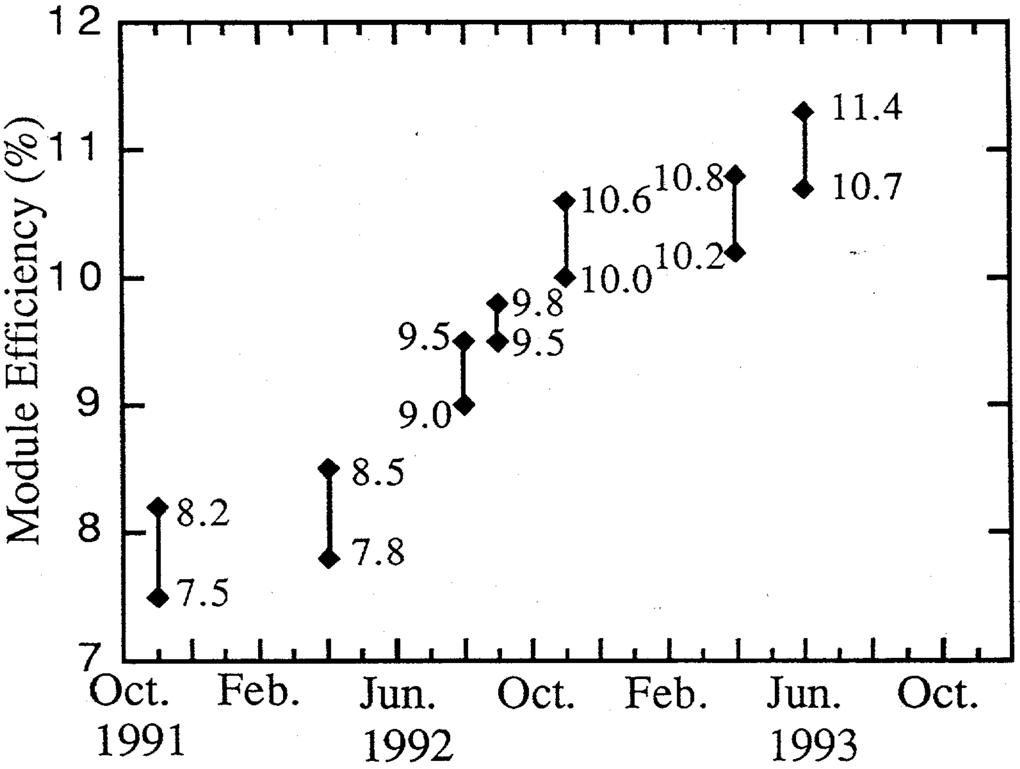

Figure 26. **Progress in double-junction module efficiency.**

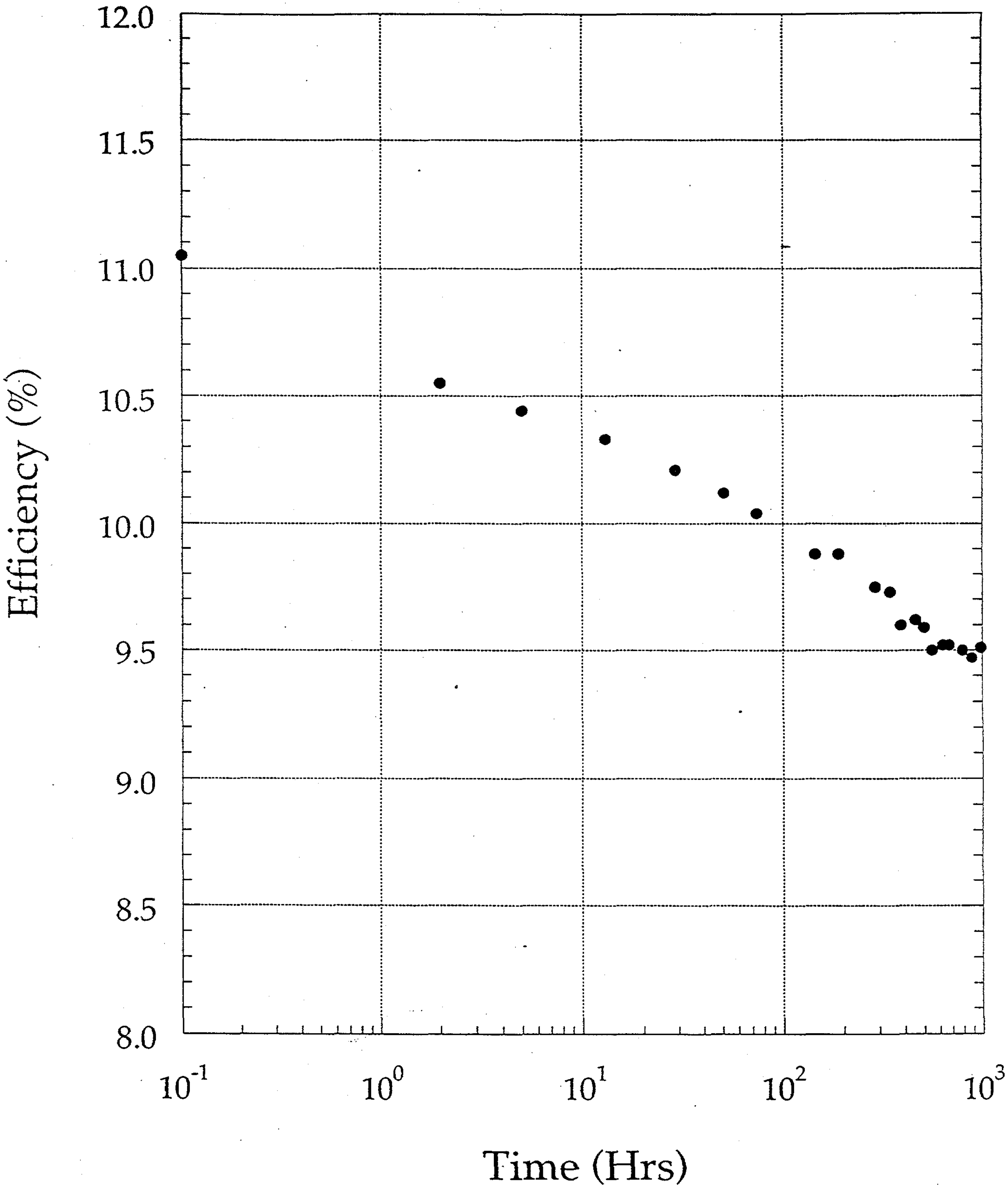

Figure 27. Light-induced degradation of double-junction module efficiency.

Table 5. **Summary of Double-Junction Module Results as Measured at NREL.**

Module No.	Efficiency (%)	
	Indoor	Outdoor
2178	11.4	10.9
2180	11.3	10.85
2185	11.4	11.0
1944	11.0	10.6

Section 5

Outdoor Efficiency Measurement

We have performed an analysis comparing module efficiency measurements made under a Spire 240A pulsed simulator and outdoors under prevailing conditions. These outdoor conditions were uncorrected for spectrum or temperature and used a global pyronometer to evaluate the total input irradiance. The indoor measurements were performed at USSC and outdoor measurements at NREL. These measurements took place over a 17-month period from spring of 1992 to August 1993.

We had found over this period of time that results evaluated on the Spire simulator showed significant and steady progress in module efficiency [Fig. 26]. At the same time, the efficiency measured on the same set of modules outdoors did not necessarily correlate with the indoor measurement, and, in fact, showed very erratic progress [Fig. 28]. Furthermore, we found that the two measurements agreed quite well in the summer and disagreed considerably in the winter. During one six-month period, the panel efficiency increased by 10% on the simulator, while the outdoor measurement showed no difference at all.

Figure 29 shows a graph of the ratio of the module efficiency measured outdoors to module efficiency measured indoors plotted versus time. The squares represent control module #1 which was measured on several occasions and stored in between measurements. The stars represent control sample #2. The solid dots each represent a different test module. It is quite obvious there is a very large seasonal variation in this ratio. This ratio peaks in August at a value near unity and has a minimum in December with values well below 90%. There was, therefore, a 15% variation in outdoor efficiency measurements with respect to simulator efficiency measurements.

Three possible explanations for the above data were considered. The first is that the Spire simulator measurement was not at all repeatable. After analyzing control sample data measured at USSC over the same period of time, it was found that the variation in output of these modules was within ± 1% of constant [Fig 30]. Therefore, the Spire simulator was indeed repeatable and was not responsible for the variation.

The second hypothesis was that the test modules were optimized differently for each set of modules. We do not believe this to be the case for two reasons: First, the control samples exhibited the same variation as the test modules, and, secondly, the variation was cyclical with season over this 17-month period.

The last hypothesis was that the outdoor prevailing conditions were fluctuating with season. To test this idea, we analyzed the spectral data measured outdoors at the time of each module measurement. What was found was that there was a large difference between the prevailing spectra and the standard spectrum for many of the measurements. What was needed then was a method to correct the outdoor data for this discrepancy in spectral distribution.

The challenge had now become what was the best correction to apply to these multijunction devices. The multijunction device inherently does not allow for a single correction to be applied. The reasoning for this is that each junction has a different spectral response, and that junction has a voltage operating point that also depends on the other junctions. Hence, even if one particular junction has been corrected properly, the relationship between junctions may result in an incorrect fill factor. This was the basis for

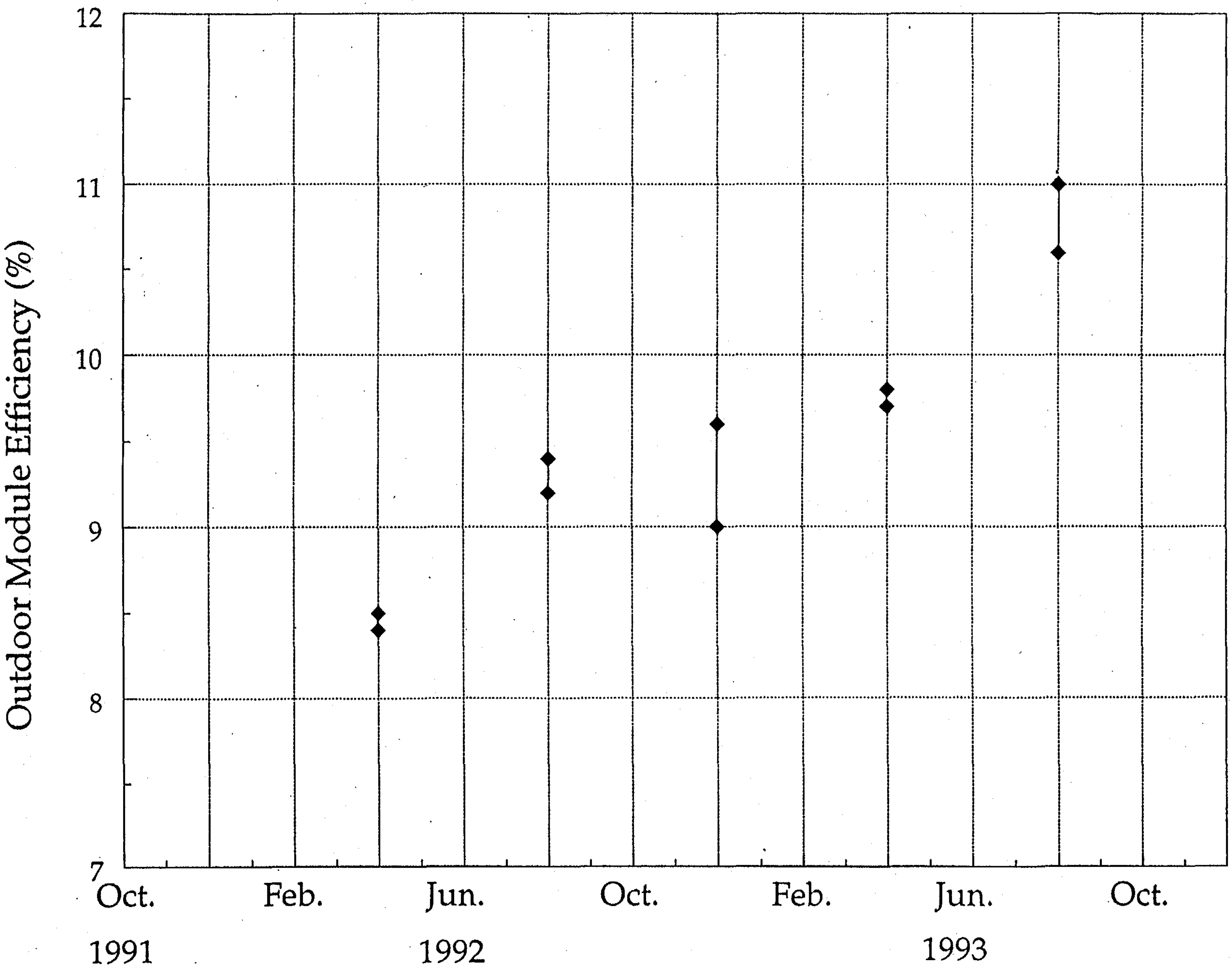

Figure 28. Progress of outdoor module efficiency versus time. Bars indicate range of efficiencies for several panels.

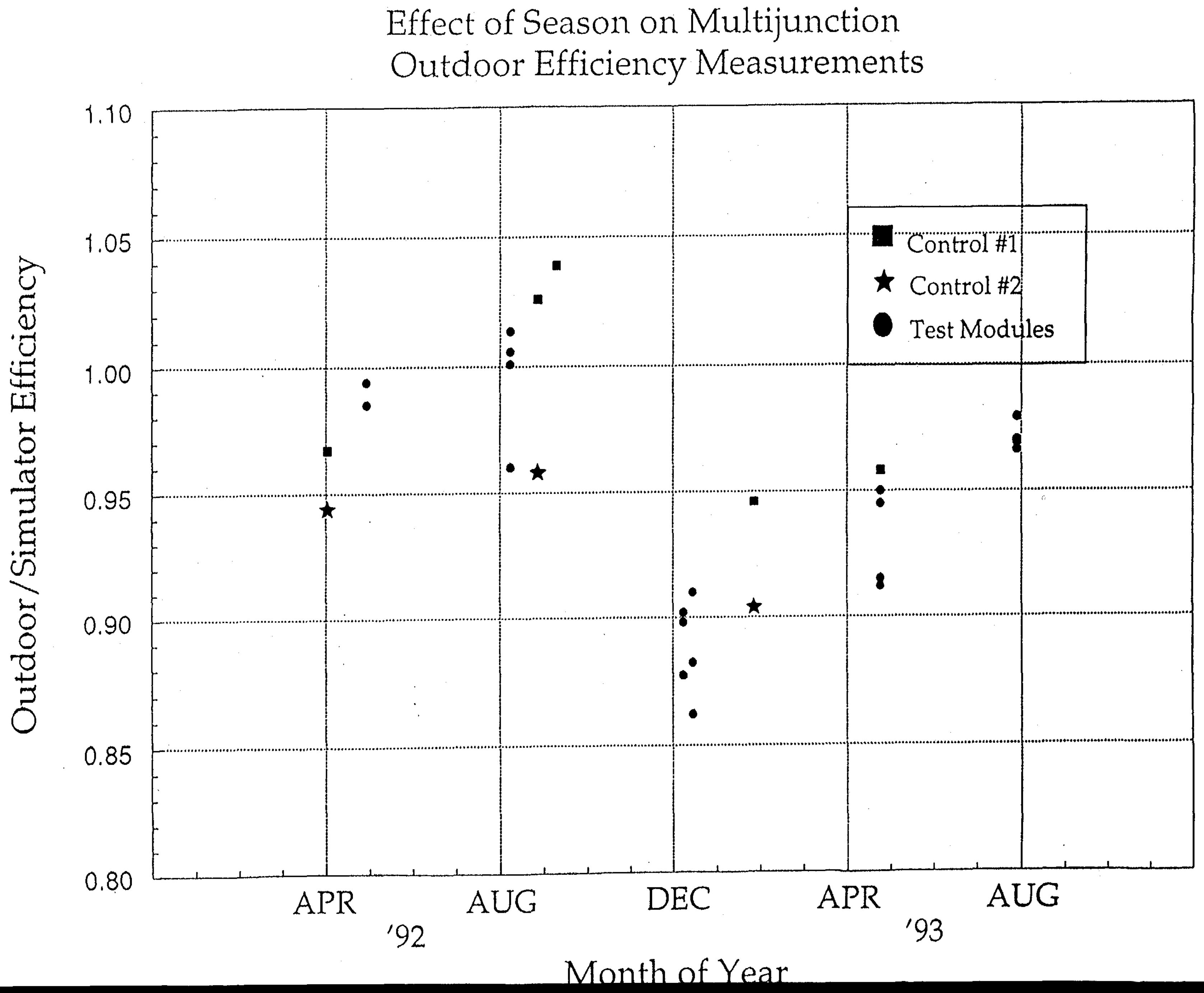

Figure 29. Plot of the ratio of outdoor to indoor module efficiency versus time of year. Squares represent control sample 1, stars control sample 2, and dots individual test modules.

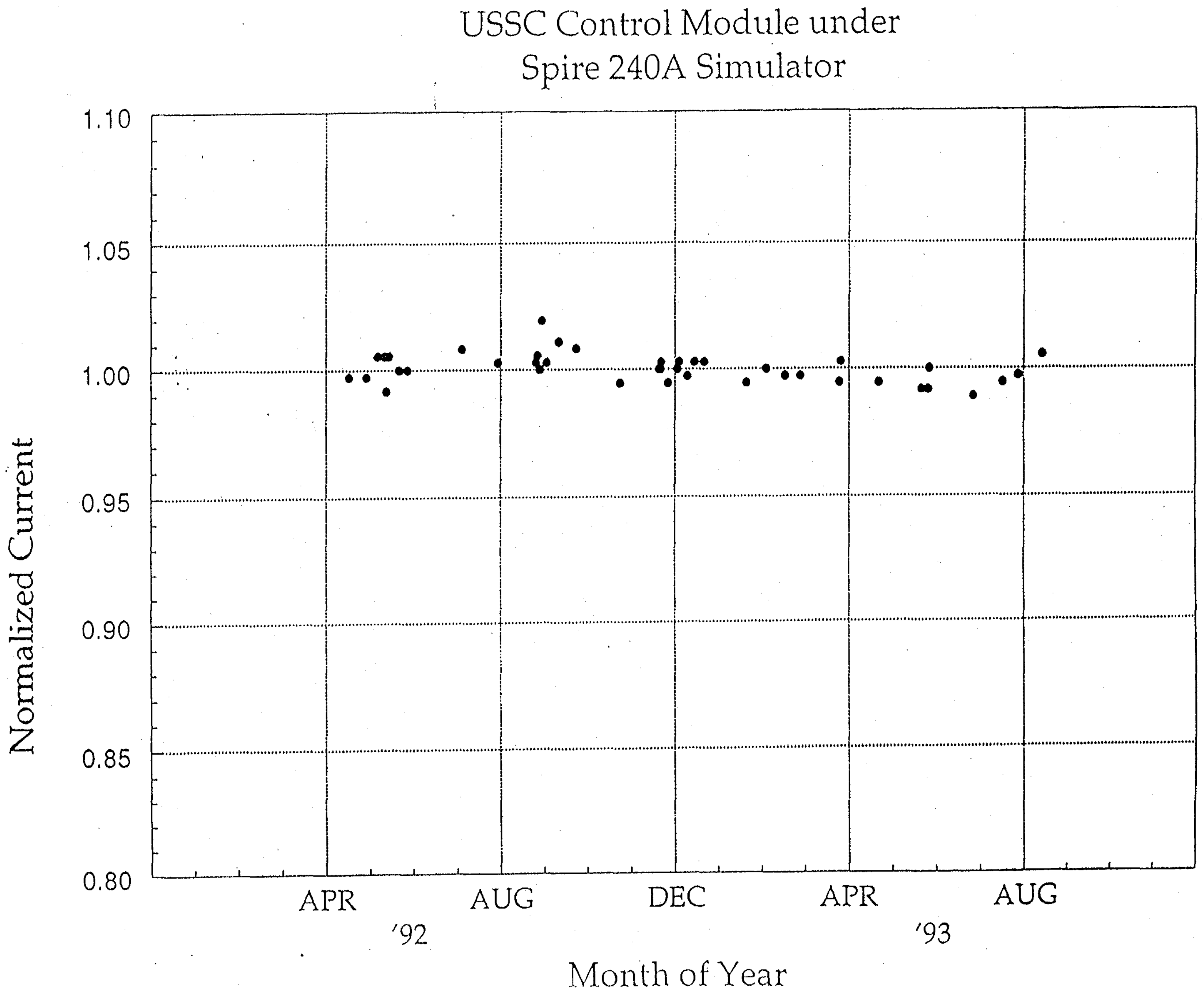

Figure 30. Output of a control module evaluated on the USSC spire simulator versus time.

developing the multisource spectral approach which enables all junctions to be properly corrected simultaneously. This obviously cannot be performed outdoors and is quite difficult to apply indoors over large areas.

The most accurate correction, as we will show, was to apply a spectral mismatch to a single-cell device that most accurately represented the response of the overall multijunction response. This was identified to be a single a-Si:Ge device with a bandgap of approximately 1.5 eV. Figure 31 shows the response of an a-Si:Ge single cell with the envelope of the multijunction response. What this achieved was that the average corrected junction current, under outdoor conditions, would now be equivalent to the average junction current under the standard spectrum. For example, the uncorrected ratio of junction current under prevailing conditions (for a December 1992 data point) to reference conditions was 0.87 and 0.91 for the top and bottom junctions, respectively. The spectral mismatch using the a-Si:Ge single-cell, for *this* case, was 0.89. If we correct the junction current by this mismatch, we arrive at corrected ratios of 0.98 and 1.02 for top and bottom, respectively. This gives an average for both junctions of 1.00.

It is still apparent that there is a mismatch between the two junctions, in the above example, with respect to the reference spectrum. This junction mismatch, with respect to the reference spectrum, will result in a different fill factor for the multijunction device under the prevailing conditions. Since the quantity of the fill factor difference will be less than the junction mismatch, we would expect the prevailing-conditions fill factor to be well within 2% of the reference fill factor. In fact, based on studies performed on a multisource simulator, the maximum change in fill factor that could be expected was 0.4 percent per percent of mismatch. As was observed, the spectral correction in this example was greater than 10% -- well in excess of the maximum 2% fill factor error. The largest ratio deviation for any point and any junction for the data in Fig. 29 after correction was ± 2.5%. Therefore, the largest error in the outdoor fill factors would be less than 2.5%.

The procedure, then, was to use the spectral irradiance measured at the time of module measurement to evaluate the spectral mismatch. The mismatch was calculated using the pyronometer as the reference device, the a-Si:Ge single-cell as the test device, the prevailing conditions spectrum as the source spectrum and the standard AM 1.5 global spectrum as the reference spectrum. The current obtained outdoors for the module was then divided by this spectral mismatch value, and efficiency subsequently calculated with this adjusted current.

In Fig. 32, we show the same plot as in Fig. 29 with the spectral correction also plotted. The control samples were not included in this graph because spectral data could not be obtained for these points. The solid circles are the "as-measured" ratios, and the open circles are the ratios corrected for the outdoor spectral data. It is quite apparent that these corrections have completely eliminated any seasonal variation in this comparison. The largest correction in this data of 12% was made in December, while the smallest correction was a small negative correction in the summer data.

There were still two questions to be answered. The first was why is the correction factor for the prevailing conditions so large and what was it due to? The second question was if using the pyronometer produces such a large correction, what would be the best reference cell to use in order to minimize this correction?

In order to properly evaluate the spectral considerations, it was first necessary to expand the wavelength range of the spectral irradiance. The spectrum was obtained using a silicon-based spectral radiometer. This meant that actual data was only obtained for a wavelength range of 300-1100 nm. The desired range for the pyronometer is from 300 to 2500 nm. To achieve this range, we fit the measured data to an atmospheric spectral model. This is a valid procedure since all parameters in the model may be obtained

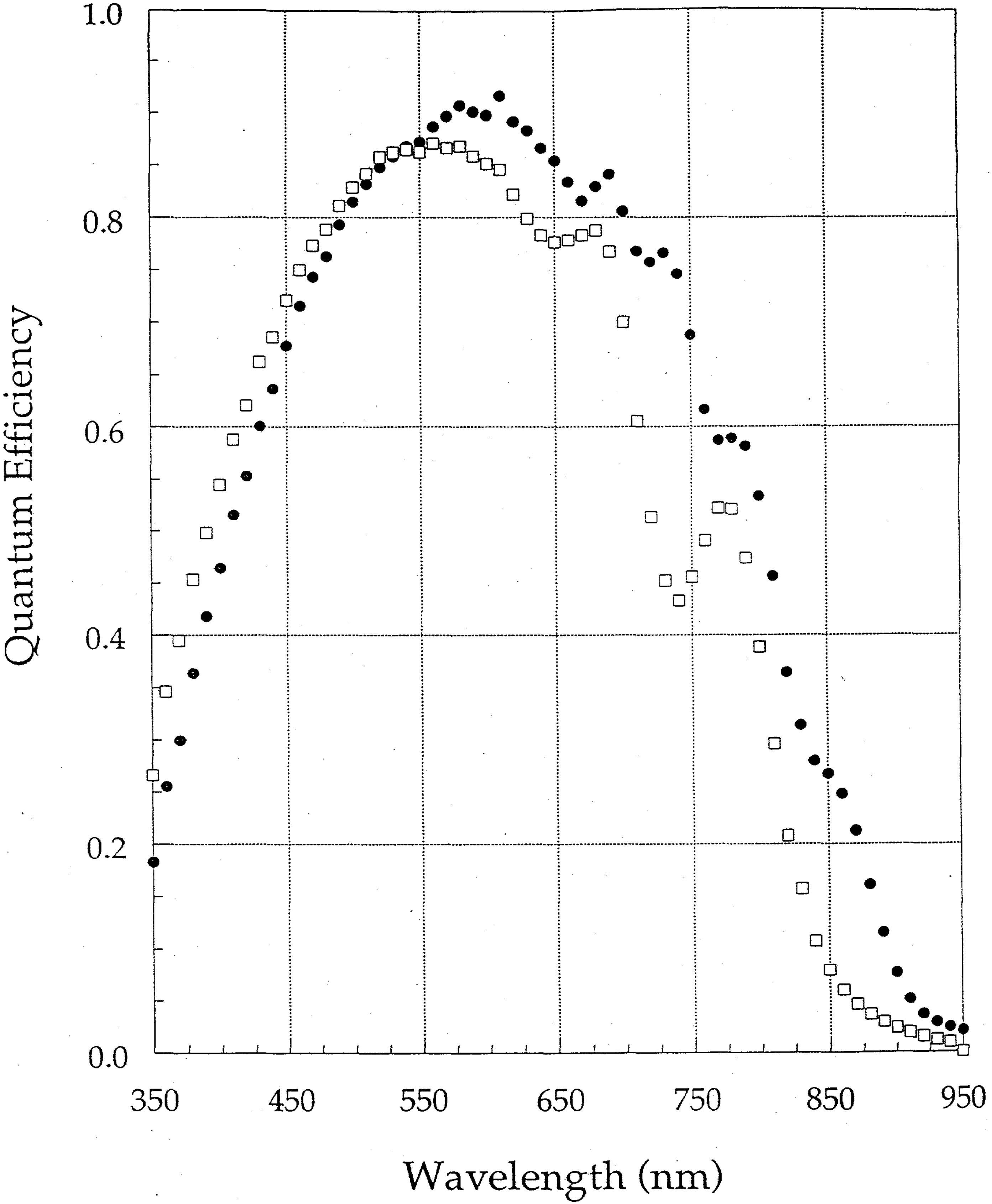

Figure 31. **Comparison of the quantum efficiency of a single a-Si:Ge device (□) used in spectral mismatch calculation to the envelope a double junction device (●).**

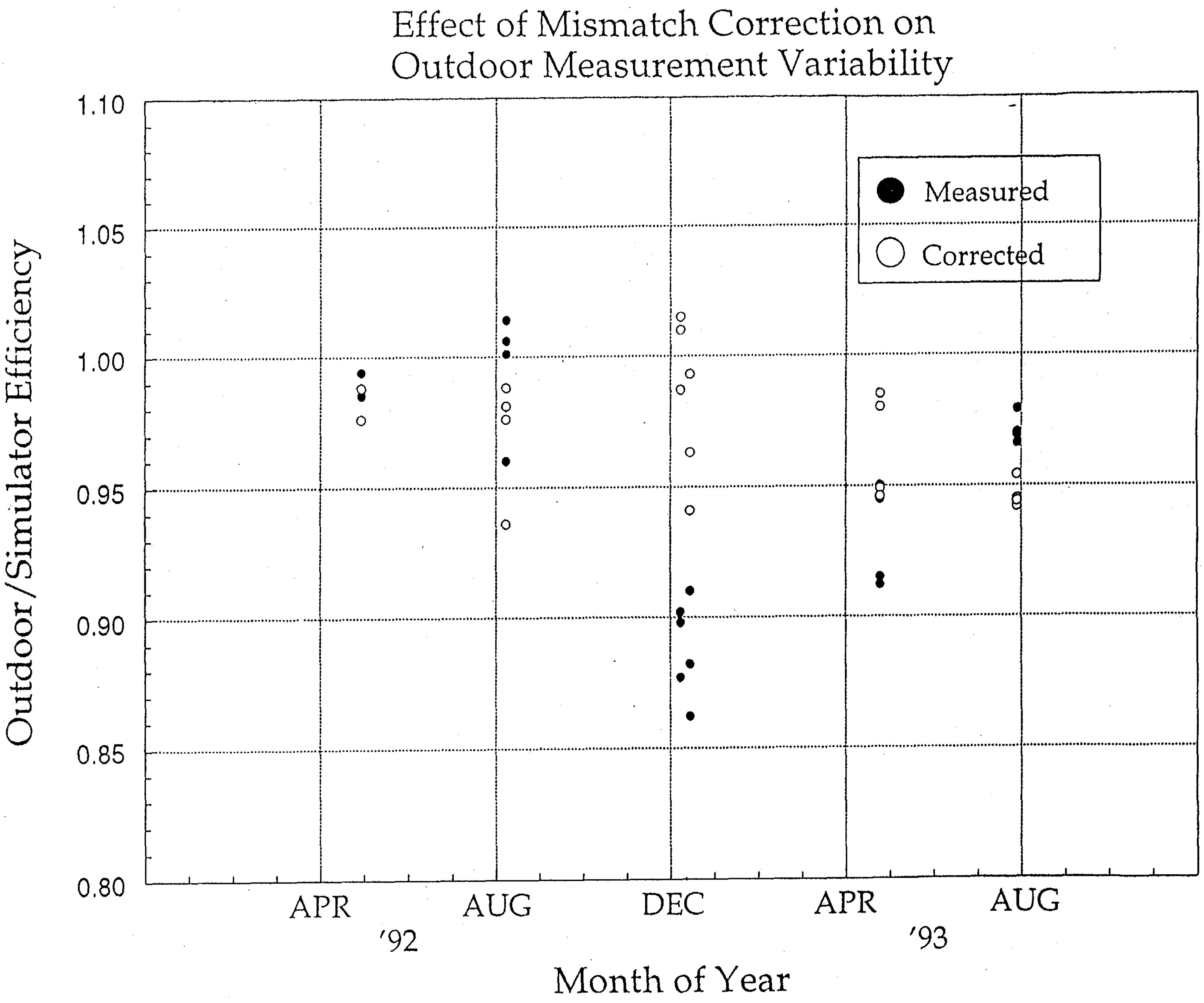

Figure 32. Plot of the ratio of outdoor to indoor module efficiency versus time of year. Solid dots represent as measured, and open dots represent spectral corrected outdoor measurements.

from the experimental data. This allowed us to calculate a spectral mismatch factor involving a pyronometer which has a response range to 2 microns. Figure 33 shows the quality of the modeled to measured fit.

Figure 34 shows a plot of the standard spectrum and the prevailing spectrum taken in April of 1992. This spectrum produced a correction factor of only 1%. It is apparent that the prevailing spectrum is a good match to the standard spectrum in this case. Figure 35 shows a plot of the standard spectrum and the prevailing spectrum taken in December of 1992. This spectrum produced a large correction factor of 12%. It is also apparent that the prevailing spectrum is a poor match to the standard spectrum primarily in the infrared portion of the spectrum. This difference is due to water vapor absorption bands and not a difference in air mass. Since these absorption bands appear only in the infrared, the pyronometer sees an additional 9% irradiance level over that of the standard spectrum, whereas the a-Si module, since it responds only to the visible, sees almost no difference between the prevailing and standard spectra. This results in a greatly underestimated efficiency for the a-Si module with respect to the global standard spectrum.

Returning to the second question, what reference device should be used in place of the pyronometer to reduce this large spectral mismatch error? To investigate this we tried five different cases, the results of which are displayed in Table 6. In each of these cases, we applied the mismatch correction to the outdoor data and calculated the mean and standard deviation for the outdoor/indoor ratio over the entire time period. The first, labeled pyronometer, was to apply no mismatch to the outdoor data of Fig. 29 (uncorrected) and use a pyronometer as the reference detector. This resulted in the average ratio of outdoor to indoor efficiency, over this time period, being 0.945 with a large standard deviation of 5.0%. The second case, labeled x-Si, was again applying no mismatch and using a x-Si module as a reference device. This resulted in a mean of the outdoor to indoor ratio of 0.942 with a larger deviation of 5.7%. The third case, labeled a-Si single, was to correct the outdoor efficiency by the spectral mismatch between the pyronometer and a single a-Si device. The mean ratio for this case was 0.970 with an improved deviation of 3.0%. The next case was to correct the outdoor measurement by the mismatch between the pyronometer and a single a-Si:Ge device. This turned out to give the smallest standard deviation of 2.1% in the ratio, while the mean was 0.970. In the final case, we adjusted the outdoor measurement by the mismatch between the pyronometer and the top cell of a double-junction device. This would have the effect, since the top cell typically limits, of only correcting for the multijunction current. This resulted in a higher deviation of 4.3% as compared to 2.1% using a single a-Si:Ge device.

Table 6. Effect of Reference Device on Outdoor Efficiency Correction.

Reference Cell Type	Mean	Deviation
Pyronometer	.945	5.0%
x-Si	.942	5.7%
a-Si single	.970	3.0%
a-Si:Ge single	.970	2.1%
a-Si top tandem cell	.961	4.3%

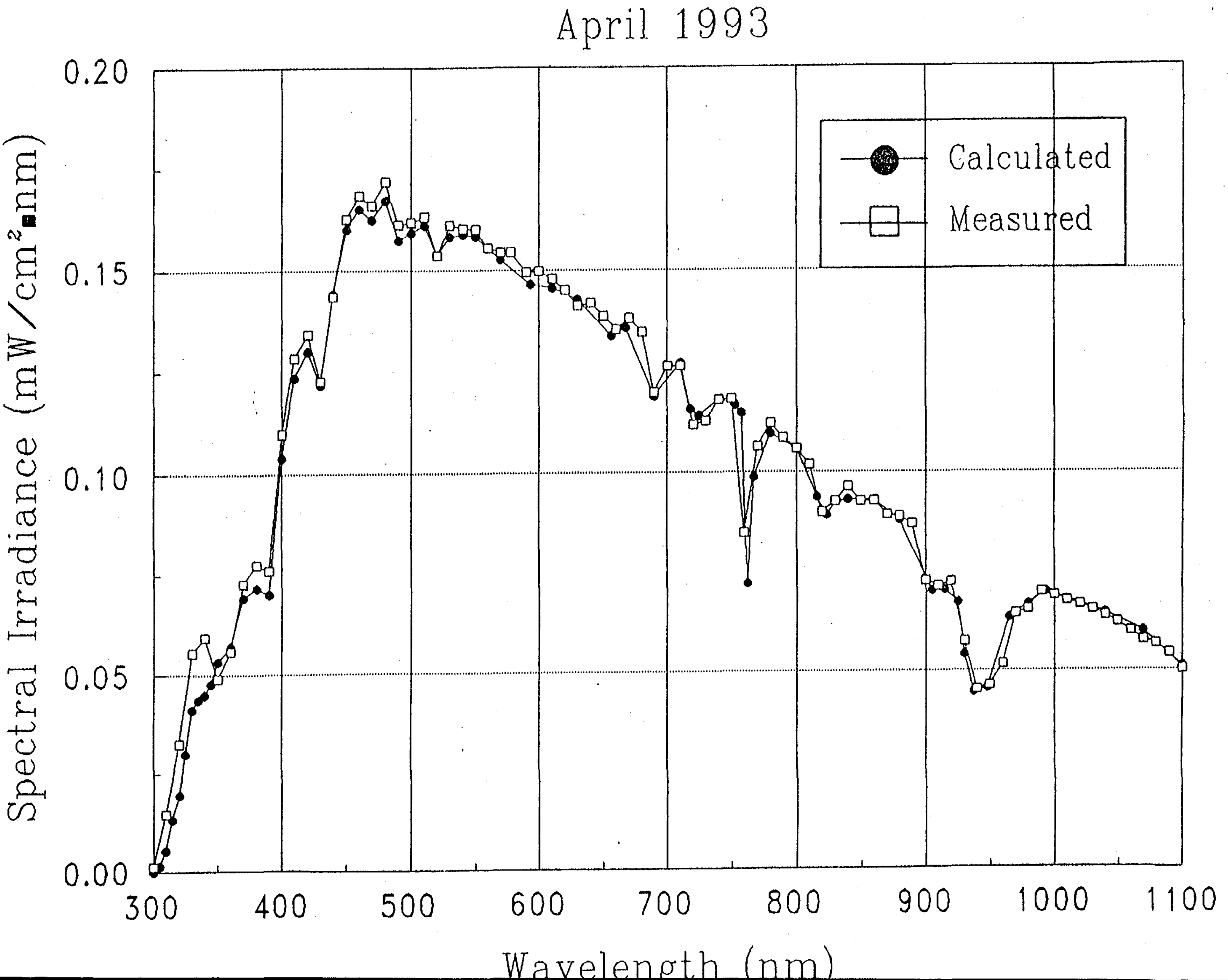

Figure 33. Comparison of the measured and curve fit spectral irradiance measured outdoors.

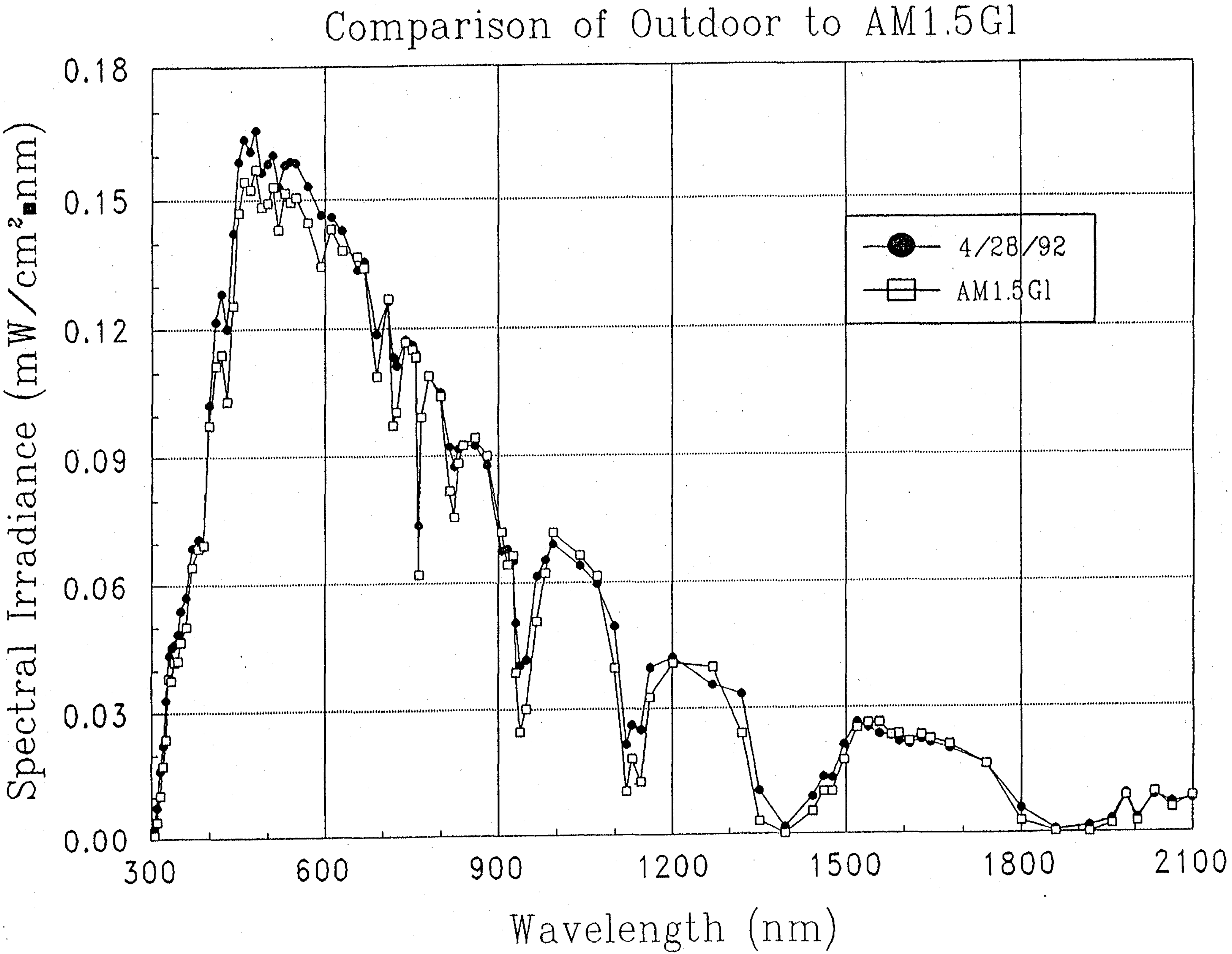

Figure 34. Plot of the standard spectrum and the prevailing spectrum taken in April of 1992.

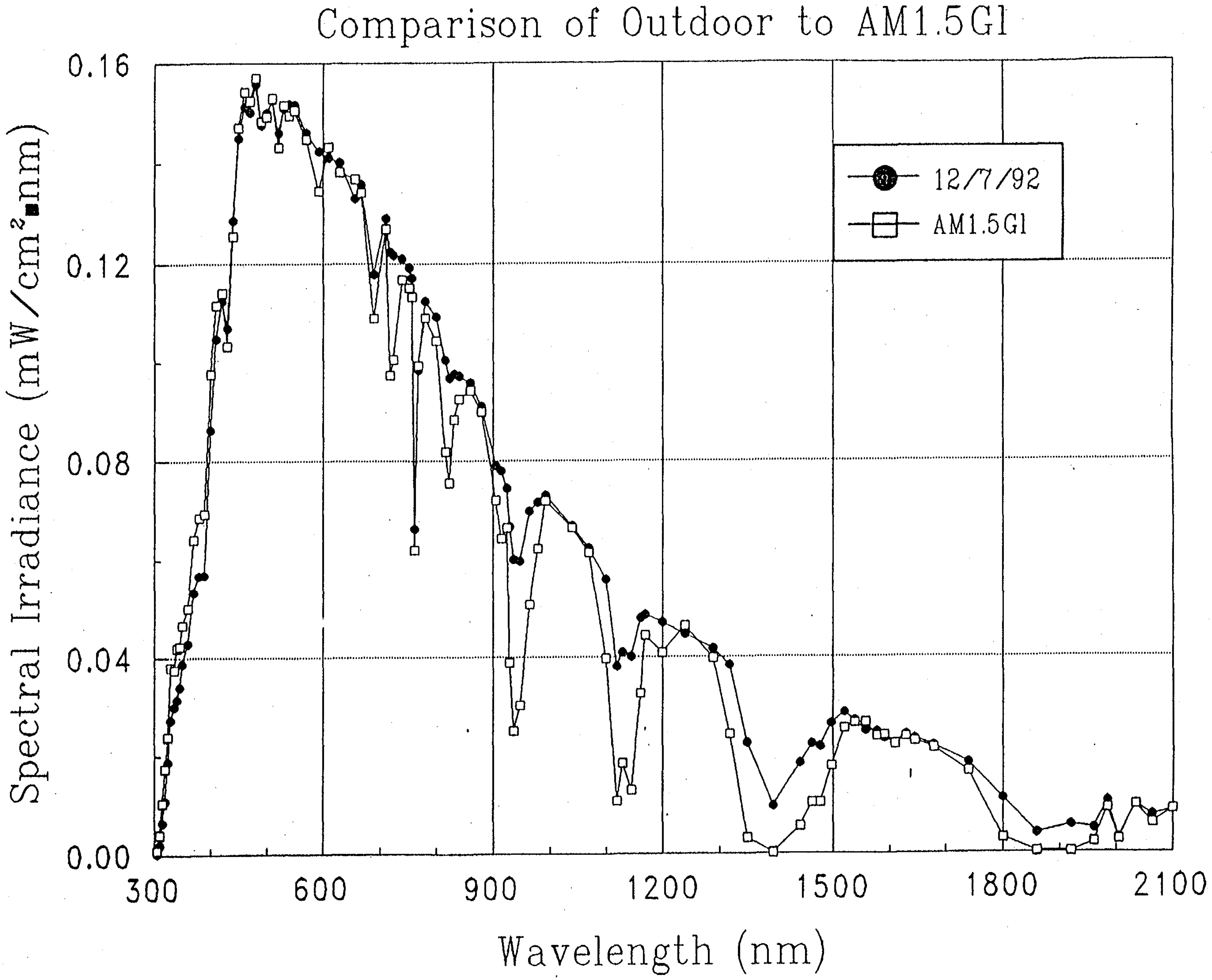

Figure 35. Plot of the standard spectrum and the prevailing spectrum taken in December of 1992.

We therefore found, from our spectral analysis, that the most appropriate reference device to evaluate the total irradiance would be an a-Si:Ge cell with a bandgap of about 1.5 eV. This device best matches the overall response of the multijunction module as can be seen from Fig. 31. We found that by using this device, we were able to reduce the scatter in the outdoor measurement from a standard deviation of ± 5% for the pyronometer to just ± 2% for the a-Si:Ge cell. In other words, if an a-Si:Ge reference device had been used to determine the original total input irradiance instead of the pyronometer, there would have been no need to correct the outdoor data in the first place.

In conclusion, we found by applying spectral mismatch corrections to outdoor efficiency measurements, we were able to reduce the standard deviation in those measurements from ± 5% to ± 2% for a-Si based multijunction modules. We also found the maximum range of spectral corrections applied to the outdoor modules efficiencies was + 12.5% for the December measurements to - 2.6% for the August measurements. Most of this correction was simply due to insufficient water vapor absorption in the prevailing spectra. We believe that it is vital that this correction procedure be applied to outdoor measurements since it both reduces the deviation significantly and is the most accurate method to date for measuring multijunction modules outdoors.

Section 6

Conclusions and Future Directions

During the period under review, significant advances have been made in obtaining higher efficiency in double-junction modules. A large number of double-junction modules have been fabricated with initial efficiencies exceeding 11%. The highest initial efficiency reached is 11.4%, as confirmed by NREL. This is the highest efficiency confirmed by NREL for any thin film module. The improvement in efficiency has been obtained through a combination of i) optimization of the individual intrinsic layers, ii) reduction in the losses at the "tunnel" junction, iii) lowering the grid and encapsulation losses and iv) better uniformity of the deposited layers over one-square-foot area. Simultaneously, through a series of fundamental studies, important information has been obtained on the microstructure of the materials and its effect on cell performance.

The highest stabilized efficiency of the double-junction modules obtained to date after light soaking for 1000 h is 9.5%. We have shown earlier that triple-junction cells not only have higher efficiency, but they have better stability too. During the next six months, we shall concentrate on fabrication of triple-junction modules which will lead us to 10% stable module efficiency.

References

1. K. Hoffman and T. Glatfelter, Proc. 23rd IEEE PV Specialists Conference, 986 (1993).
2. S. Guha, Annual Report, ZM-1-19033-2 (National Renewable Energy Laboratory, Golden, CO, 1993).
3. A. Smith, A. Rohatgi, and S. Neel, Proc. 21st IEEE PV Specialists Conference, 426 (1990).
4. E. Yablonovitch and G. Cody IEEE Trans. Ed-29, 300 (1982).
5. T. Sawada, H. Tarui, N. Terada, M. Tanaka, T. Takahama, S. Tsuda, and S. Nakano, Proc. 23rd IEEE PV Specialists Conference, 803 (1993).
6. X. Xu, J. Yang, and S. Guha, Proc. 23rd IEEE PV Specialists Conference, 971 (1993).
7. Y. M. Li, Proc. Mat. Res. Soc. Symp. Proc. **297**, 803 (1993).
8. S. Guha, Final Report, SERI/TP-211-3918, (National Renewable Energy Laboratory, Golden, CO, 1990).
9. A. Pawlikiewicz and S. Guha, IEEE Trans. ED-37, 403 (1990).
10. H. R. Park, J. Z. Liu, P. Roca i Cabarrocas, A. Maruyama, S. Wagner, J. R. Abelson, and F. Finger, Appl. Phys. Lett. **57**, 1440 (1990).
11. S. Guha, K. L. Narasimhan, and S. M. Pietruszko, J. Appl. Phys. **52**, 859 (1981).
12. K. Tanaka and A. Matsuda, Mat. Sci. Report **2**, 139 (1987).
13. D. A. Doughty, J. R. Doyle, G. H. Lin, and A. Gallagher, J. Appl. Phys. **67**, 6220 (1990).
14. S. Guha, J. Yang, S. J. Jones, Y. Chen, and D. L. Williamson, Appl. Phys. Lett. **61**, 1444 (1992).
15. J. Yang, R. Ross, T. Glatfelter, R. Mohr, G. Hammond, C. Bernotaitis, E. Chen, J. Burdick, M. Hopson, and S. Guha, Proc. 20th IEEE PV Specialists Conference, 241 (1988).
16. S. Guha, J. Yang, P. Nath, and M. Hack, Appl. Phys. Lett. **49**, 218 (1986).
17. S. J. Jones, Y. Chen, D. L. Williamson, R. Zedlitz, and G. Bauer, Appl. Phys. Lett. (to be published).
18. S. J. Jones, Y. Chen, D. L. Williamson, X. Xu, J. Yang, and S. Guha, Mat. Res. Soc. Symp. Proc. **297**, 815 (1993).
19. Q. Wang, H. Antoniadis, E. A. Schiff, and S. Guha, Mat. Res. Soc. Symp. Proc. **258**, 881 (1992).

Document Control Page	1. NREL Report No. NREL/TP-411-6396	2. NTIS Accession No. DE94000298	3. Recipient's Accession No.

4. Title and Subtitle

Research on Stable, High-Efficiency Amorphous Silicon Multijunction Modules

5. Publication Date

March 1994

6.

7. Author(s)

S. Guha

8. Performing Organization Rept. No.

9. Performing Organization Name and Address

United Solar Systems Corporation
Troy, Michigan

10. Project/Task/Work Unit No.

PV431101

11. Contract (C) or Grant (G) No.

(C) ZM-1-19033-2

(G)

12. Sponsoring Organization Name and Address
National Renewable Energy Laboratory
1617 Cole Blvd.
Golden, CO 80401-3393

13. Type of Report & Period Covered

Technical Report
1 March 1993 - 30 November 1993

14.

15. Supplementary Notes
NREL technical monitor: W. Luft

16. Abstract (Limit: 200 words)

This report describes the progress made during the first half of Phase III of the R&D program to obtain high-efficiency amorphous silicon alloy multijunction modules. The highlight of the work includes (1) demonstration of the world's highest initial module efficiency (area of 0.09 m^2) of 11.4% as confirmed by NREL, and (2) demonstration of stable module efficiency of 9.5% after 1-sun light soaking for 1000 h at 50°C. In addition, fundamental studies were carried out to improve material properties of the component cells of the multijunction structure and to understand the optical losses associated with the back reflector.

17. Document Analysis
a. Descriptors
high efficiency ; amorphous silicon ; multijunction ; modules ; photovoltaics ; solar cells

b. Identifiers/Open-Ended Terms

c. UC Categories
271

18. Availability Statement
National Technical Information Service
U.S. Department of Commerce
5285 Port Royal Road
Springfield, VA 22161

19. No. of Pages

68

20. Price

A04

Form No. 0069E (6-30-87)